

## Chapter 2

# Surface-Layer Properties and Parameterizations

Footprint models are generally based both on parameterizations and simplified assumptions typically for the lower atmospheric boundary layer. For the experimentalist in need of footprint models, it is important to know the spatial extent and the range of atmospheric conditions of each footprint model so that the most appropriate one can be selected for the purpose at hand. This chapter therefore introduces the reader to the concept of atmospheric boundary layer and parameterizations, linking those to footprint models where these parameterizations are used. More details can be found in textbooks and in relevant papers (Stull 1988; Garratt 1992; Kaimal and Finnigan 1994; Arya 1999, 2001; Hatfield and Baker 2005; Foken 2008; Monteith and Unsworth 2008; Wyngaard 2010; Moene and van Dam 2014).

### 2.1 Atmospheric Boundary Layer and Scales

The atmospheric boundary layer is the lowest layer of the troposphere near the ground where the friction decreases with height. In that layer, the wind velocity decreases significantly from the geostrophic wind above the boundary layer to the wind near the surface and the wind direction changes counter-clockwise on the Northern hemisphere by up to  $30^{\circ}$ – $45^{\circ}$ . The upper boundary is a mostly static stable layer (inversion) characterized by intermittent turbulence. The exchange processes between the atmospheric boundary layer and the free troposphere take place in the entrainment zone (Fig. 2.1). The thickness of this layer is approximately 10 % of the atmospheric boundary layer, which has a thickness of about 1–2 km over land and 0.5 km over the oceans. In strong stable stratification, its thickness can be as little as 10 m.

In addition, the diurnal cycles of solar radiation, temperature, humidity, and wind are also highly variable (Stull 1988), see Fig. 2.2. After sunrise, the atmosphere is warmed up by the heat transported from the surface upward and the inversion layer created during the night breaks up. The new layer is very turbulent, well mixed (mixed layer) and topped by the entrainment zone. Shortly before sunset, the stable (nightly) boundary layer develops near the ground. It has the

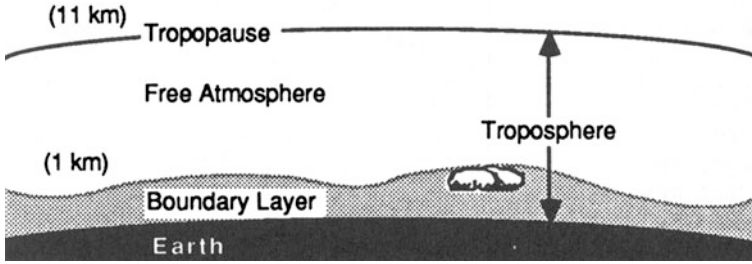


**Fig. 2.1** The troposphere and its two parts: the atmospheric boundary layer and the free atmosphere (Stull 2000)

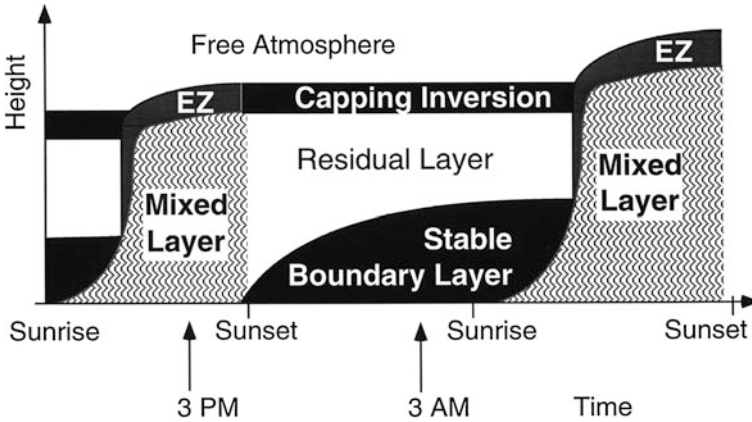


**Fig. 2.2** Daily cycle of the structure of the atmospheric boundary layer (Stull 2000), EZ Entrainment zone

characteristics of a surface inversion and spans only approximately 100 m in depth. Above this layer, the mixed layer of the day is not very turbulent and is called the residual layer. The latter is capped by a free (capping) inversion—the upper border of the boundary layer (Seibert et al. 2000). At sunrise, the growing mixed layer rapidly erodes both the stable boundary layer and the residual layer. On overcast days, the life time of the residual layer is longer and the boundary layer is more layered than during sunny convective days.

On days with high solar irradiation, the layer structure is destroyed by convective cells. These occupy relatively small updrafts areas and develop typically over larger areas with uniform surface heating in relation to the surrounding areas like land-lake or dry-wet areas. This is according to modeled studies over areas larger than 200–500 m (Shen and Leclerc 1995).

In the upper boundary layer (*upper layer*, *Ekman layer*) the change of wind direction takes place in the lowest 10 %. That region is called the *surface* or the *Prandtl layer* (Fig. 2.3). Its height is approximately 20–50 m in the case of

height in m	name		exchange		stability
1000	upper layer (Ekman-layer)		turbulent	no constant flux	influence of stability
20	turbulent layer	surface layer (Prandtl- layer)		flux nearly constant with height	no influence of stability
1	dynamic sublayer				
0.01	viscous sublayer				
0.001	laminar/ molecular boundary layer				

Fig. 2.3 Structure of the atmospheric boundary layer (Foken 2008)

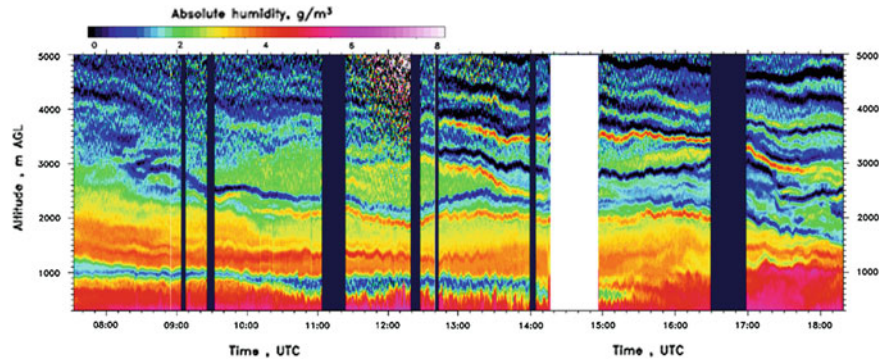
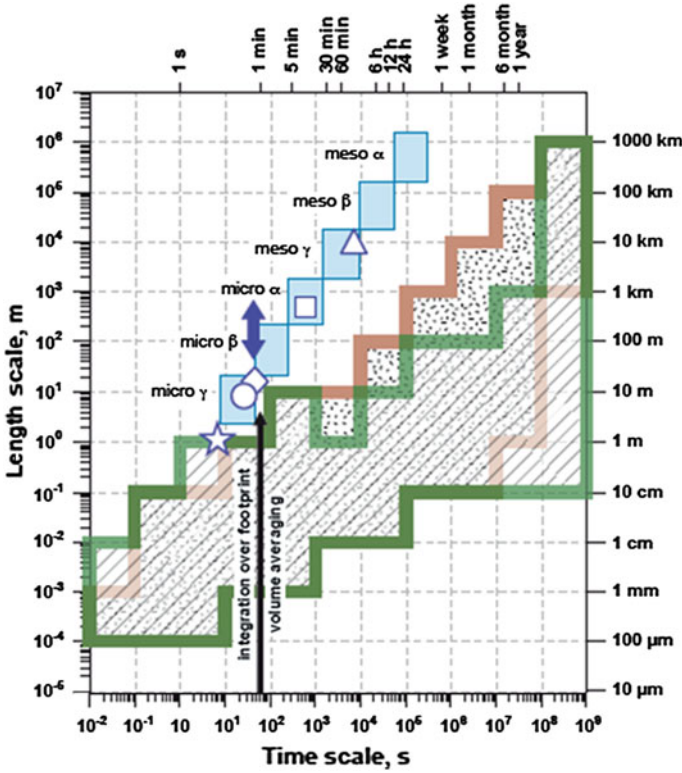


Fig. 2.4 Highly variable structure of the atmospheric boundary layer and of the boundary layer height measured with a Lidar (Behrendt et al. 2009, Published with kind permission of © International Society for Optics and Photonics, 2009. All Rights Reserved)

unstable conditions and a few meters in stable stratification. It is also called the *constant flux layer* because of the assumption of nearly constant fluxes with height. In this layer, the vertical wind profile is logarithmic (*inertial sublayer*). This assumption forms the basis of similarity theory, first attributed to Monin and Obukhov (1954). Because of this height invariance in energy and mass fluxes, these fluxes can be measured anywhere within the surface layer. The very thin *viscous* and *laminar* (term used for the flow field) or *molecular layer* (term used for scalars), is not very relevant for measurements but nevertheless used in several models (Fig. 2.3). According to the similarity theory by Monin and Obukhov (1954), a layer with a thickness of approximately 1 m (*dynamical sublayer*) is not influenced by atmospheric stability—this layer is nearly always neutral. In the real atmosphere the atmospheric boundary layer is highly variable (Fig. 2.4), which can partly described in footprint models (Kljun et al. 2002; Steinfeld et al. 2008).

Atmospheric processes are characterized by time scales extending from seconds (e.g. turbulent exchange) to several days (e.g. Rossby waves, horizontal



**Fig. 2.5** Temporal and spatial scales of atmospheric (turbulent), plant (physiological), and soil processes. Atmospheric processes (Orlanski 1975) are given in *light blue squares* of one order of magnitude (from micro  $\gamma$  to meso  $\alpha$ ). Forest canopy related transport processes comprise turbulent transport in canopy (*white star*), vertical advection in canopy (*white circle*), transport above canopy (*white diamond*), coherent structures (*blue double arrow*), footprint averaged turbulent flux (*white square*), and horizontal advection at canopy top (*white triangle*). The scales of plant processes, relevant for energy and matter exchange with the atmosphere (Schoonmaker 1998), is the spotted area, those of soil processes (Blöschl and Sivapalan 1995; Vogel and Roth 2003) are shown by the brown framed (Foken et al. 2012, designed by E. Falge, modified, Published with kind permission of © Copernicus Publications, distributed under the Creative Commons Attribution 3.0 License, 2012. All Rights Reserved)

advection), and from millimetres (e.g. smallest eddies) to the size of high and low pressure areas (up to  $10 \times 10 \text{ km}^4$ ). For atmospheric processes, scales (defined e.g. by Orlanski 1975) range between  $10^0$ – $10^7 \text{ m}$  and  $10^0$ – $10^6 \text{ s}$ , respectively (see Fig. 2.5, diagonal orientated boxes). Atmospheric scales of exchange processes of energy and mass related to the issue of this book comprise both turbulent transport and coherent structures inside and above canopies, footprint-related turbulent fluxes, and horizontal advection in and at the canopy top in a range between  $10^0$ – $10^4 \text{ m}$  and  $10^0$ – $10^4 \text{ s}$ , respectively.

In contrast, soil and plant processes cover similar time scales but smaller length scales. While flux measuring methods (like the eddy-covariance technique) are working in the typical atmospheric scale mainly the micro- $\alpha$ ,  $\beta$ ,  $\gamma$  scales dependent on the measuring height, the footprint method is a tool to average the smaller soil and plant scales with the atmospheric scales typically on the micro- $\alpha$ ,  $\beta$  scale. This is in a simplified format shown in Fig. 2.5. Because most footprint models assume a homogeneous surface, special area-averaging techniques must be used, which is a topic of Sect. 2.5.

## 2.2 Turbulence Parameterization

Footprint models rest on the assumptions of vertical profiles of wind, temperature and scalar as well as profiles of turbulence parameters. These depend on fluxes of momentum, sensible and latent heat or on the concentration of trace gases. Since turbulence variables are often limited, they must be parameterized using other meteorological data. The basis for this lies in the typical similarity or simplifications of the latter. The most important is the flux-profile similarity and the flux-variance similarity. The first is identical with the Monin-Obukhov similarity theory (Monin and Obukhov 1954; Foken 2006), which expresses the relationship between the turbulent flux and the vertical gradient of its state parameter and the gradient of the wind velocity under the assumption of a stratified surface layer. A more simple relation is the well-known logarithmic profile according to Prandtl (1925) in neutral conditions. Both can be simplified using the Bowen-ratio similarity (Bowen 1926), i.e. the ratio of two fluxes is proportional to the difference of its state parameters between two levels mathematically. The flux-variance similarity describes the relation between the turbulent flux and the variance of the state parameter (Obukhov 1960) which is often also a function of stability in the surface layer. Both similarity relations will be described below in addition to often used empirical functions. The similarity theory based on the assumption of horizontal homogeneity, low vegetation, and steady state conditions. These assumptions are often not fulfilled and limit the application of footprint models, as turbulence properties and variables are typically inhomogeneous in the nature.

### 2.2.1 Flux-Gradient Similarity

According to Prandtl (1925) and its mixing length theory for neutral conditions, the turbulent fluxes follow the flux-gradient similarity or the so-called  $K$ -approach. In general terms,  $K$  represents the sum of the molecular diffusion and the turbulent diffusion coefficient. Because the turbulent coefficient is up to five orders of magnitude larger than the molecular coefficient, only the latter is used. This however does not apply to the viscous sublayer. The turbulent fluxes are

proportional to the gradient of the state variable with the turbulent diffusion coefficient  $K$ . Therefore, the momentum flux  $\tau$ , the sensible heat flux  $Q_H$  and the mass flux  $Q_\chi$  (for water vapour the latent heat flux  $Q_E$ ) are

$$\tau = \rho u_*^2 = -\rho \overline{u'w'} = \rho K_m \frac{\partial \bar{u}}{\partial z} \quad (2.1)$$

$$Q_H = c_p \rho \overline{w'T'} = -c_p \rho K_H \frac{\partial \bar{T}}{\partial z} \quad (2.2)$$

$$Q_\chi = \rho \overline{w'\chi'} = -\rho K_\chi \frac{\partial \bar{c}}{\partial z} \quad (2.3)$$

where  $K_m$ ,  $K_H$  and  $K_\chi$  are the turbulent diffusion coefficients for momentum, sensible heat and trace gases,  $\rho$  is the air density,  $c_p$  is the specific heat for constant pressure,  $u$  is the horizontal wind velocity,  $T$  is the temperature,  $c$  is the trace gas concentration and  $w'$ ,  $u'$ ,  $T'$  and  $c'$  are the turbulent fluctuations of the vertical and horizontal wind components, the temperature and the trace gas concentration. The equation for the friction velocity  $u_*$  is only valid, if  $u$  is aligned in the direction of the mean wind velocity. This can be expressed in Cartesian coordinate as

$$u_* = \left[ (\overline{u'w'})^2 + (\overline{v'w'})^2 \right]^{1/4}, \quad (2.4)$$

where are  $\overline{u'w'}$  and  $\overline{v'w'}$  are the two components of the momentum tensor in the direction of the horizontal wind components  $u$  and  $v$  and  $\overline{w'T'}$  and  $\overline{w'c'}$  are the temperature and concentration flux with the vertical wind component  $w$ , the temperature  $T$  and the concentration of a trace gas (e.g. water vapour)  $c$ . The averaging operator obeys the Reynolds averaging of the total flux

$$\overline{xw} = \bar{x} \bar{w} + \overline{x'w'}, \quad (2.5)$$

where  $x$  can be replaced by the variable of the mean quantity of interest and  $x'$  the instantaneous component. Because of the assumption that  $\bar{w} = 0$ , the total flux can be replaced by the turbulent flux, which can be measured as a covariance  $\overline{x'w'}$  (with the eddy-covariance method). This assumption is far from trivial, since it is seldom fulfilled for several reasons in the surface layer including surface heterogeneity, vegetation, topography, or instrumental reasons (Aubinet et al. 2012). To realize this, the coordinate system must be rotated into the streamlines (Kaimal and Finnigan 1994; Wilczak et al. 2001; Finnigan et al. 2003). Furthermore, there are instances in the stable boundary layer where Eq. 2.5 must see the addition of a wave component (Foken and Wichura 1996; Durden et al. 2013). The wave component is embedded in the signal and is superimposed to the turbulent flux.

The relation between the turbulent diffusion coefficient for momentum  $K_m$  and heat  $K_H$  is given by the turbulent Prandtl number

$$K_m = \text{Pr}_t \cdot K_H \quad (2.6)$$

which is  $\text{Pr}_t \sim 0.8$ . The relation between the turbulent diffusion coefficients of momentum and water vapour is called the turbulent Schmidt number  $Sc_t$ . In the case of neutral stratification,  $K_m$  can be written according to the concept of the flow near the wall with the von-Kármán constant  $\kappa$  (Prandtl 1925):

$$K_m = \kappa \cdot z \cdot u_* \quad (2.7)$$

Combining these relations expressing the turbulent diffusion coefficients with Eqs. (2.1)–(2.3), the equations for the friction velocity, the sensible and the latent heat flux can be expressed in kinematic units, where  $q$  is the specific humidity:

$$u_* = \sqrt{-\overline{u'w'}} = \kappa \cdot z \cdot \frac{\partial u}{\partial z} = \kappa \cdot \frac{\partial u}{\partial \ln z} \quad (2.8)$$

$$\overline{w'T'} = -\frac{1}{\text{Pr}_t} \cdot \kappa \cdot u_* \cdot \frac{\partial T}{\partial \ln z} \quad (2.9)$$

$$\overline{w'q'} = -\frac{1}{Sc_t} \cdot \kappa \cdot u_* \cdot \frac{\partial q}{\partial \ln z} \quad (2.10)$$

The turbulent fluxes of sensible heat can be transferred into energetic units by multiplication with the air density for dry air (pressure  $p$  in hPa and temperature in K)

$$\rho = \frac{p \cdot 100}{287.0586 \cdot T} \text{ [kgm}^{-3}\text{]}. \quad (2.11)$$

For wet air, the air temperature must be replaced by the virtual temperature

$$T_v = T(1 + 0.61 \cdot q), \quad (2.12)$$

which includes the influence of moisture on air density. The heat capacity for constant pressure is

$$c_p = 1004.832 \text{ [JK}^{-1}\text{kg}^{-1}\text{]}. \quad (2.13)$$

The latent heat flux in energetic units follows the multiplication of Eq. (2.10) with air density and the specific heat of evaporation

$$\lambda = 2500827 - 2360(T - 273.15) \text{ [Jkg}^{-1}\text{]}. \quad (2.14)$$

If the latent heat flux in kinematic units were not determined with the specific humidity but instead with water vapour pressure, an additional multiplication with the factor  $\frac{0.622}{p}$ , where  $p$  is in hPa, is necessary.

**Table 2.1** Roughness length in m from different sources (Reithmaier et al. 2006, updated)

surface	ESDU (1972)	Troen and Peterson (1989)	Wieringa (1992)	Fiedler according to Hasager and Jensen (1999)	Davenport et al. (2000)
Ice	$10^{-5}$				
Water	$10^{-4}$ – $10^{-3}$				
Snow	0.002				
Bare soil		0.03	0.004	0.03	0.005
Grassland	0.005–0.02	0.03	0.06	0.08	0.03
Winter crops (winter)		0.1	0.09	0.12	0.1
Winter crops	0.05	0.1	0.18	0.09	0.25
Summer crops	0.05	0.1	0.18	0.09	0.25
Clearings		0.1	0.35	0.004	0.2
Shrubs	0.2	0.4	0.45	0.3	0.5
Conifer forest	1–2	0.4	1.6	0.9	1.0
Deciduous forest	1–2	0.4	1.7	1.2	2.0
Settlement	0.5–2	0.4	0.7	0.5	2.0

Furthermore, for heights above approximately 10 m, the temperature must be replaced in all equations given above by the potential temperature

$$\theta = T \left( \frac{1000}{p} \right)^{R_L/c_p}. \quad (2.15)$$

The integration of Eq. (2.8) is given by

$$u(z) - u(z_0) = u_* \ln \frac{z}{z_0}, \quad (2.16)$$

where  $z_0$  is an integration constant. Because this parameter is dependent on the characteristics of the underlying surface, it is called the roughness parameter or the roughness length. It varies from  $10^{-3}$  to  $10^{-5}$  m for water and ice,  $10^{-2}$  m for grassland up to 0.2 m for small trees. More data are given in Table 2.1. Additional details about the application of the different schema are given in Sect. 6.2.1.

The integration of the equations for the sensible (2.9) and the latent heat (2.10) flux is formally identical to those of the momentum flux. The integration constants are so-called roughness temperature  $z_{0T}$  and roughness humidity  $z_{0q}$ . Both are approximately 10 % of the roughness length. In this region, the temperature and the humidity have approximately the value of those near the surface. These roughness lengths are usually parameterized in models.



$$T(z) - T(z_{0T}) = -\frac{\text{Pr}_t \cdot T_*}{\kappa} \ln \frac{z}{z_{0T}} \quad (2.17)$$

$$q(z) - q(z_{0q}) = -\frac{\text{Sc}_t \cdot q_*}{\kappa} \ln \frac{z}{z_{0q}} \quad (2.18)$$

with the dynamical temperature or temperature scale

$$T_* = -\frac{\overline{w'T'}}{u_*} \quad (2.19)$$

and the dynamical moisture scale

$$q_* = -\frac{\overline{w'q'}}{u_*}. \quad (2.20)$$

The extension of the profile equation for non-neutral conditions is given by Monin-Obukhov's similarity theory (Monin and Obukhov 1954). This theory defines a dimensionless Obukhov parameter

$$\zeta = z/L \quad (2.21)$$

which describes the effects of friction, sensible heat flux and buoyancy. The parameter  $L$  is called Obukhov length (Obukhov 1946, 1971; Businger and Yaglom 1971; Foken 2006).

$$L = -\frac{u_*^3}{\kappa \frac{g}{T} \frac{Q_H}{\rho \cdot c_p}} \quad (2.22)$$

This definition is valid near the surface and provides low moisture content. In the case that air density is influenced by moisture, the use of the virtual temperature is more exact, Eq. (2.12). In addition, the temperature should be replaced by virtual temperature in the air density Eq. (2.12). The more exact definition of the Obukhov length is with the virtual potential temperature:

$$L_v = -\frac{u_*^3}{\kappa \frac{g}{\theta_v} \frac{Q_{Hv}}{\rho \cdot c_p}}. \quad (2.23)$$

In this equation,  $Q_{Hv}$  is called the buoyancy flux because it includes also the motion due to the moisture effect on air density. The buoyancy flux can be determined with Eq. (2.9) by replacing the temperature by the virtual temperature, which is nearly equal to the sonic temperature (Kaimal and Gaynor 1991) measured with sonic anemometers (Sect 7.2).

**Table 2.2** Determination of the stability the surface layer dependent on the dimensionless parameter  $\zeta$  and the universal function  $\varphi(\zeta)$  adopted from Foken (2008)

Stability	Remark	$\zeta$	$\varphi(\zeta)$
Unstable	Free convection, independent from $u_*$	$-1 > \zeta$	No definition
	Dependent from $u_*$ , $T_*$	$-1 < \zeta < 0$	$\varphi(\zeta) < 1$
Neutral	Dependent from $u_*$	$\zeta \sim 0$	$\varphi(\zeta) = 1$
Stable	Dependent from $u_*$ , $T_*$	$0 < \zeta < 0.5 \dots 2$	$1 < \varphi(\zeta) < 3 \dots 5$
	Independent from $z$	$0.5 \dots 1 < \zeta$	$\varphi(\zeta) \sim \text{const} \sim 3 \dots 5$

From the application of Monin-Obukhov similarity theory on profiles, Eqs. (2.8)–(2.10), follows a dependency on the dimensionless parameter  $\zeta$  (Table 2.2), which is the basis of the universal functions  $\varphi_m(\zeta)$ ,  $\varphi_H(\zeta)$  and  $\varphi_E(\zeta)$  for the momentum, sensible and latent heat exchange:

$$u_* = \sqrt{-\overline{u'w'}} = \frac{\kappa \cdot z}{\varphi_m(\zeta)} \cdot \frac{\partial u}{\partial z} = \frac{\kappa}{\varphi_m(\zeta)} \cdot \frac{\partial u}{\partial \ln z} \quad (2.24)$$

$$\overline{w'T'} = -\frac{\kappa \cdot u_*}{\text{Pr}_t \cdot \varphi_H(\zeta)} \cdot \frac{\partial T}{\partial \ln z} \quad (2.25)$$

$$\overline{w'q'} = -\frac{\kappa \cdot u_*}{\text{Sc}_t \cdot \varphi_E(\zeta)} \cdot \frac{\partial q}{\partial \ln z}. \quad (2.26)$$

The present recommendation for the use of universal functions (Fig. 2.6) is the universal functions by Businger et al. (1971) in the re-evaluated form by Högström (1988). Given that several footprint models use other functions, a selection is given in Table 2.3 for momentum flux and Table 2.4 for the sensible and latent heat fluxes. There is a paucity of universal functions for the stable stratification because of the complexity of the nocturnal stable boundary layer (Andreas 2002). The universal functions can be assumed to be constant for  $\zeta > 0.8$  (see e.g. Handorf et al. 1999).

The accuracy of the profile method depends on those of the turbulent Prandtl or Schmidt numbers, the von-Kármán constant and the universal functions. For the turbulent Prandtl number, an overview of data several authors is given in Table 2.5. The von-Kármán constant is presently accepted as  $\kappa = 0.40 \pm 0.01$  (Högström 1996). For the universal function, the following accuracies are given by Högström (1996):

$$\begin{aligned}
|z/L| \leq 0.5 : & \quad |\delta\varphi_H| \leq 10 \% \\
|z/L| \leq 0.5 : & \quad |\delta\varphi_m| \leq 20 \% \\
z/L > 0.5 : & \quad \varphi_m, \varphi_H = \text{const} ?
\end{aligned} \quad (2.27)$$

**Table 2.3** Universal function for the momentum exchange including the re-evaluated form by Högström (1988) with a von-Kármán constant of 0.40 and marked with \*, adapted from Foken (2008)

References	$\kappa$	Universal function for momentum exchange, $\varphi_m(\zeta)$	
Webb (1970)	–	$1 + 4.5 z/L$	$z/L < -0.03$
Businger et al. (1971)	0.35	$(1 - 15 z/L)^{-1/4}$	$-2 < z/L < 0$
		$1 + 4.7 z/L$	$0 < z/L < 1$
Businger et al. (1971), Högström (1988)	0.40*	$(1 - 19.3 z/L)^{-1/4}$	$-2 < z/L < 0$
		$1 + 6 z/L$	$0 < z/L < 1$
Dyer (1974)	0.41	$(1 - 16 z/L)^{-1/4}$	$-1 < z/L < 0$
		$1 + 5 z/L$	$0 < z/L$
Dyer (1974), Högström (1988)	0.40*	$(1 - 15.2 z/L)^{-1/4}$	$-1 < z/L < 0$
		$1 + 4.8 z/L$	$0 < z/L$

**Table 2.4** Universal function for the exchange of sensible and latent heat including the re-evaluated form by Högström (1988) with a von-Kármán constant of 0.40 and marked with \*, adapted from Foken (2008)

References	$\kappa$	Universal function for the exchange of sensible and latent heat	
Webb (1970)	–	$1 + 4.5 z/L$	$z/L < -0.03$
Businger et al. (1971)	0.35	$0.74 (1 - 9 z/L)^{-1/2}$	$-2 < z/L < 0$
		$0.74 + 4.7 z/L$	$0 < z/L < 1$
Businger et al. (1971), Högström (1988)	0.40*	$0.95 (1 - 11.6 z/L)^{-1/2}$	$-2 < z/L < 0$
		$0.95 + 7.8 z/L$	$0 < z/L < 1$
Dyer (1974)	0.41	$(1 - 16 z/L)^{-1/2}$	$-1 < z/L < 0$
		$1 + 5 z/L$	$0 < z/L$
Dyer (1974), Högström (1988)	0.40*	$0.95(1 - 15.2 z/L)^{-1/2}$	$-1 < z/L < 0$
		$0.95 + 4.5 z/L$	$0 < z/L$

For the re-evaluation by Högström (1988) use  $\varphi_H(\zeta) \sim \varphi_E(\zeta)$ ,  $Pr_t = Sc_t = 1$  because both numbers are already included into the universal function

It must be assumed that surface-layer parameterizations are influenced by boundary-layer conditions, specially by those of the mixed-layer height (Johansson et al. 2001). It should be pointed out however that the influence of the latter is still second to the influence of atmospheric stratification.

Integrating Eqs (2.24) and (2.26) and using the universal functions presented in Tables 2.3 and 2.4 was first shown by Paulson (1970). The integration from the roughness length  $z_0$  to  $z$  in the wind profile applies the definition  $u(z_0) = 0$

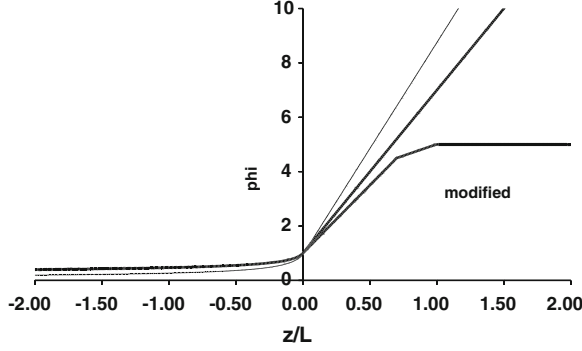


**Fig. 2.6** Typical universal function for momentum (*bold line*) and the heat and mass exchange (*thin line*). The line ‘modified’ uses a height-independent range (Foken 2008). Well defined is the function only in the range  $|z/L| < 1$  (Tables 2.2, 2.3, and 2.4)

**Table 2.5** The reciprocal turbulent Prandtl number according to different authors (Foken 2008)

Authors	$Pr_t^{-1}$
Businger et al. (1971)	1.35
– correction according to Wieringa (1980)	1.00
– correction according to Högström (1988)*	1.05
Kader and Yaglom (1972)	1.15–1.39
Foken (1990)	1.25
Högström (1996)	$1.09 \pm 0.04$

\*Högström (1988) uses  $Pr_t = 1$  in the profile equation, but has included  $Pr_t = 1.05$  in the universal function (see Tables 2.3 and 2.4)

$$\begin{aligned}
 u(z) - u(z_0) &= u(z) = \frac{u_*}{\kappa} \left[ \ln \frac{z}{z_0} - \int \phi_m(z/L) dz \right] \\
 u(z) &= \frac{u_*}{\kappa} \left[ \ln \frac{z}{z_0} - \psi_m(z/L) \right]
 \end{aligned} \tag{2.28}$$

with the integrated universal function:

$$\psi_m(\varsigma) = \int_{z_0/L}^{z/L} [1 - \phi_m(\varsigma)] \frac{d\varsigma}{\varsigma}. \tag{2.29}$$

The integration of the universal function by Businger et al. (1971) and subsequently reformulated by Högström (1988) is for the momentum exchange and the flux of sensible heat in the unstable case:

$$\psi_m(\varsigma) = \ln \left[ \left( \frac{1+x^2}{2} \right) \left( \frac{1+x}{2} \right)^2 \right] - 2 \tan^{-1} x + \frac{\pi}{2} \quad \text{for } \varsigma < 0 \tag{2.30}$$

$$\psi_H(\varsigma) = 2 \ln \left( \frac{1+y}{2} \right) \quad \text{for } \varsigma < 0 \quad (2.31)$$

with

$$x = (1 - 19.3\varsigma)^{1/4} \quad y = 0.95 (1 - 11.6\varsigma)^{1/2}. \quad (2.32)$$

In the stable case, the integration is very simple:

$$\psi_m(\varsigma) = -6\varsigma \quad \text{for } \varsigma \geq 0 \quad (2.33)$$

$$\psi_H(\varsigma) = -7.8\varsigma \quad \text{for } \varsigma \geq 0. \quad (2.34)$$

As far as other universal functions are concerned, according to Tables 2.3 and 2.4, the parameters  $x$  and  $y$  in Eq. (2.32) must be defined differently.

Besides the stability parameter,  $\varsigma$  represents also another stability parameter which can be formulated using the equation of turbulent energy (TKE). The ratio of the buoyancy production term and the mechanical production term is called the flux Richardson number (Richardson 1920; Stull 1988)

$$Ri_f = \frac{g}{T} \cdot \frac{\overline{w'T'}}{\overline{w'u'} \cdot \left( \partial u / \partial z \right)}. \quad (2.35)$$

Because fluxes are proportional to gradients, a gradient Richardson number can also be defined:

$$Ri_g = - \frac{g}{T} \cdot \frac{\partial T / \partial z}{\left( \partial u / \partial z \right)^2}. \quad (2.36)$$

A further simplification is the bulk Richardson number

$$Ri_b = - \frac{g}{T} \cdot \frac{\Delta T \cdot \Delta z}{(\Delta u)^2}, \quad (2.37)$$

used in the meteorology. In analogy to the Obukhov length, the Richardson number definition can also be given using the potential and virtual temperatures. If fluxes are available, the Richardson flux number should be used. Otherwise, the gradient or bulk number will be substituted.

The critical Richardson number, which characterizes the change from turbulent to laminar or molecular conditions, is  $Ri_{gc} = 0.2$  or  $R_{fc} = 1.0$ . The recalculation from  $\varsigma$  into  $Ri_g$  is stability dependent according to the following relations (Businger et al. 1971; Arya 2001):

**Table 2.6** Overview of different stability parameters (Foken 2008), added by the potential temperature  $\theta(z) = T(0 \text{ m}) + 0.0098 \text{ K} \cdot z$ 

Stability	Temperature for $z < 10 \text{ m}$	Potential temperature	$Ri$	$L$	$\zeta = z/L$
Unstable	$T(0) > T(z)$	$\Theta(0) > \Theta(z)$	$< 0$	$< 0$	$< 0$
Neutral	$T(0) \sim T(z)$	$\Theta(0) \sim \Theta(z)$	$\sim 0$	$\pm \infty$	$\sim 0$
Stable	$T(0) < T(z)$	$\Theta(0) < \Theta(z)$	$0 < Ri_g < 0.2$ $0 < Ri_f < 1.0$	$> 0$	$0 < \zeta < \sim 1$

$$\begin{aligned} \zeta &= Ri_g \quad \text{für} \quad Ri_g < 0 \\ \zeta &= \frac{Ri_g}{1 - 5 Ri_g} \quad \text{for} \quad 0 \leq Ri_g \leq 0.2 = Ri_c. \end{aligned} \quad (2.38)$$

An overview over different parameters is given in Table 2.6.

### 2.2.2 Profile Functions Above the Canopy

Over dense vegetation (forests, crops, etc.) due to the logarithmical wind profile the surface according to Eq. (2.16) is an apparent surface at height  $d$  (displacement height, zero-plane displacement height), for which the wind profile fulfil these equations. The new height is called the aerodynamic height  $z'(d) = 0$ . In contrast, the geometric height is measured from the ground surface, is  $z = z' + d$ . Because Eq. (2.16) is valid for the aerodynamic heights (Fig. 2.7), the equation with geometric heights measured from the surface is given as:

$$u(z) = \frac{u_*}{\kappa} \ln \frac{z - d}{z_0}. \quad (2.39)$$

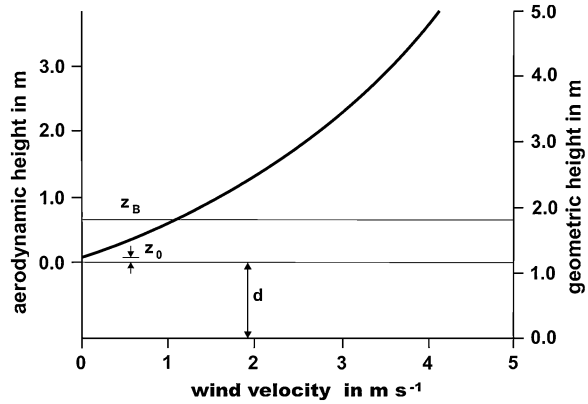
Consequently, all profile equations and equations related to integral turbulence characteristics in the following chapters must be modified for vegetation by replacing “ $z$ ” with “ $z + d$ ” or by assuming that all heights are aerodynamic heights. Usually,  $d = 0.67 h_c$  is applied with  $h_c$  as canopy height. Under these conditions, the roughness length is simply approximated by

$$z_0 = 0.1 h_c. \quad (2.40)$$

Foken (2008) recommended to determine the canopy height using the tallest plants or trees that cover 10 % or more of the vegetation at the site.

More complicated is the determination of the displacement height in an urban surface. If profile and flux measurements are available, the displacement height can be calculated using the constant flux layer assumption within the surface layer. This is referred to as the aerodynamic approach. Thereby, the displacement height

**Fig. 2.7** Aerodynamic and geometric height for dense vegetation ( $d = 1.2$  m) according to Foken (2008)



is the level where fluxes from both profile and flux measurements become identical. The displacement height can also be determined using two scintillometers placed at two different levels (Kanda et al. 2002).

The morphometric method (Grimmond and Oke 1999) has been more often used, in the simplest way

$$d = f_d \overline{z_H}, \quad z_0 = f_o \overline{z_H} \quad (2.41)$$

with  $\overline{z_H}$  as averaged building height and using the above given values of  $f_d = 0.67$  and  $f_o = 0.1$  or  $f_d = 0.8$  for densely built-up cities (Roth et al. 2006).

Another method was proposed by MacDonald et al. (1998) who use also the density of the buildings as well as the mean building height

$$d = \overline{z_H} [1 + \alpha^{-\lambda_P} (\lambda_P - 1)] \quad (2.42)$$

with empirical coefficient  $\alpha = 4.43$  and  $\lambda_P$  the plain area fraction calculated as the area fraction occupied by built-up elements.

Another approach was introduced by Raupach (1994), which uses the frontal areal index  $\lambda_F$

$$d = \overline{z_H} \left( 1 - \frac{1 - e^{-\sqrt{c_{dI} \lambda_F}}}{\sqrt{c_{dI} \lambda_F}} \right) \quad (2.43)$$

with the empirical coefficient  $c_{dI} = 7.5$ .

### 2.2.3 Profile Functions in the Canopy

Measurements of profile functions in low vegetation are very rare because of experimental problems. The sensors are often large in relation to the canopy height

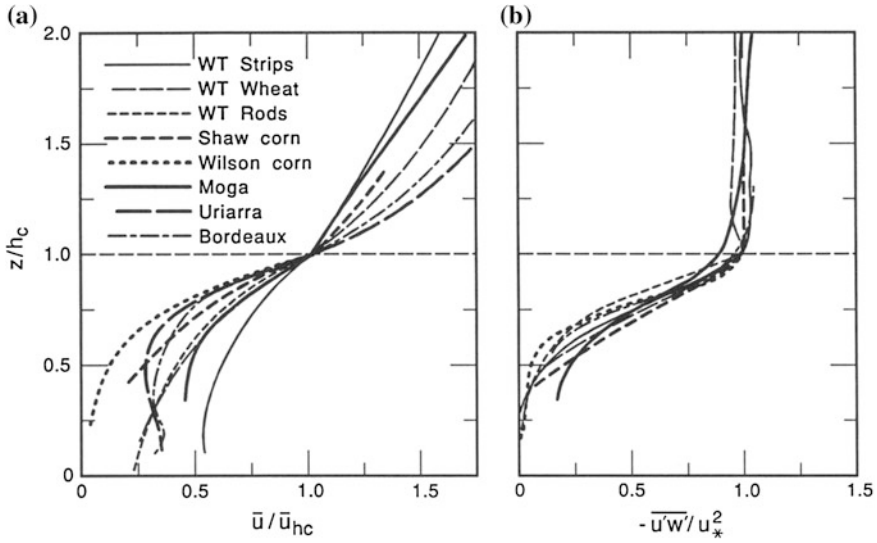


**Fig. 2.8** Profile of the mean wind velocity and the momentum flux in the canopy normalized with the value at the top of the canopy from wind tunnel, corn and forest measurements by different authors (Kaimal and Finnigan 1994): Wind tunnel (WT) shrips, Raupach et al. (1986); wind tunnel wheat, Brunet et al. (1994); wind tunnel rods, Seginer et al. (1976); Shaw corn (Shaw et al. 1974); Wilson corn (Wilson et al. 1982); moga, Raupach et al. (1996); uriarra, Denmead and Bradley (1987); Bordeaux forest, Brunet personal communication (Published with kind permission of © Oxford University Press, 1994. All Rights Reserved)

and are partly ventilated. Some examples are given by Geiger et al. (2009). For tall vegetation and for forests, much more data is available. By normalizing the profiles with their respective values at the top of the canopy, the profiles are similar to those inside a wind tunnel, in low vegetation and even in forest canopies (Fig. 2.8). Cionco (1978) proposed a profile function which depends on canopy height  $h_c$

$$\overline{u(z)} = \overline{u(h_c)} \cdot e^{\alpha(z/h_c - 1)} \quad (2.44)$$

and a coefficient  $\alpha$  given for different plants in Table 2.7.

A direct calculation of the coefficient  $\alpha$  that is vegetation type dependent is provided to us by Goudriaan (1977). The formulation of the coefficient is a function of both the mean distance of the leaves ( $l_m$ ), and the leaf area index ( $LAI$ ):

$$\alpha \cong \left( \frac{0.2 \cdot LAI \cdot h_c}{l_m} \right). \quad (2.45)$$



**Table 2.7** Values of the profile parameter  $\alpha$  in a plant canopy according to Eq. (2.45)

Plant canopy	Profile parameter $\alpha$	References
Wheat	2.45	Cionco (1978)
	1.6	Brunet et al. (1994)
Corn	1.97	Cionco (1978)
	2.4	Shaw et al. (1974)
	4.1	Wilson et al. (1982)
Rice	1.62	Cionco (1978)
Sunflower	1.32	Cionco (1978)
Larch plantation	1.00	Cionco (1978)
Forest, 20 m	1.7	Denmead and Bradley (1987)

### 2.2.4 Roughness Sublayer

Above the canopy, the profiles of the state parameters are strongly influenced by the roughness of the surface and the ideal profile (Eqs. (2.24)–(2.26)) must be modified. This range is called the roughness sublayer and includes the canopy height. It is approximately three times the canopy height. The roughness sublayer was firstly found in laboratory experiments (Raupach et al. 1980) and later in the natural environment e.g. by Shuttleworth (1989). This variable is of considerable significance to flux measurements, especially when using profile functions. While over low vegetation, typical relations of the measuring height to the roughness length  $z/z_0$  are 100–1,000. Above a forest canopy with a generally significant roughness sub-layer, that dimensionless value hovers around 5–10 (Garratt 1980).

Therefore, the Monin-Obukhov similarity assumption cannot be applied in the roughness sublayer of thickness  $z_*$  (Garratt 1978, 1980; Raupach et al. 1980; Raupach and Legg 1984), which according to Verhoef et al. (1997) is

$$z_* = h_c + cL_s \quad (2.46)$$

where  $h_c$  is the canopy height,  $c$  is 2 for momentum and 3 for heat exchange (Mölder et al. 1999) and  $L_s$  is the characteristic length scale (shear scale) of the mixing layer (Raupach et al. 1996; Finnigan 2000):

$$L_s = \frac{u(h_c)}{\left(\partial u / \partial z\right)_{z=h_c}}. \quad (2.47)$$

In their model, Rannik et al. (2003) assumed the roughness sublayer high as  $h_c + d$ , where  $d$  is the zero plane displacement of  $d = 2/3 h_c$ . In this layer, weaker gradients are found but the turbulent transport occurs largely through the action of coherent structures in the mixing layer (Raupach et al. 1996; Finnigan 2000). Therefore, an additional function  $\varphi_*(z/z_*)$  must be added to the profile equations

(Eqs. (2.24)–(2.26) to represent the effect of the roughness sublayer, since the latter increases the diffusion coefficient (Garratt 1992):

$$u_* = \sqrt{-\overline{u'w'}} = \frac{\kappa}{\varphi_{*u}(z/z_*) \cdot \varphi_m(\zeta)} \cdot \frac{\partial u}{\partial \ln z} \quad (2.48)$$

$$\overline{w'T'} = \frac{\text{Pr}_t^{-1} \cdot \kappa \cdot u_*}{\varphi_{*T}(z/z_*) \cdot \varphi_H(\zeta)} \cdot \frac{\partial T}{\partial \ln z} \quad (2.49)$$

$$\overline{w'q'} = \frac{Sc_t^{-1} \cdot \kappa \cdot u_*}{\varphi_{*q}(z/z_*) \cdot \varphi_E(\zeta)} \cdot \frac{\partial q}{\partial \ln z} \quad (2.50)$$

where  $1/\varphi_*(z/z_*)$  is called the enhancement factor (Raupach and Legg 1984; Simpson et al. 1998). The universal function for the roughness sublayer for the wind variables is given by

$$\varphi_{*u}(z/z_*) = \exp[-0.7(1 - z/z_*)] \quad (2.51)$$

(Garratt 1992; Graefe 2004). Another definition was given by Cellier and Brunet (1992)

$$\varphi_{*u} = \left(\frac{z}{z_*}\right)^\eta \quad (2.52)$$

where  $\eta = 0.6$ , which was also found by Mölder et al. (1999). The functions for scalars are not well defined. Mölder et al. (1999) found a linear relation with height for humidity and temperature i.e.

$$\varphi_{*T,q} = z/z_*. \quad (2.53)$$

Another more sophisticated method to describe this phenomenon which takes into account the coherent structures is the mixing-layer theory (Raupach et al. 1996; Finnigan 2000). This theory suggests that the reduced gradients above the top of the canopy can be attributed to the presence of Kelvin-Helmholtz instability present in strong shear flows and by the generation of disturbances and coherent structures. This approach has not yet been used in footprint analysis. A combination of both was given by Harman and Finnigan (2007, 2008), who defined the roughness sublayer for momentum and scalar fluxes dependent on the mixing layer length scale  $L_s$ , Eq. (2.47). According to this theory, both the displacement height and roughness length vary with stability.

### 2.2.5 Power Laws

For many applied purposes, power laws are used to determine the wind profile in the surface layer and the lower boundary layer (Doran and Verholek 1978; Sedefian 1980; Joffre 1984; Wieringa 1989; Hsu et al. 1994):

$$\frac{u_1}{u_2} = \left( \frac{z_1}{z_2} \right)^p. \quad (2.54)$$

In wind power applications, an exponent  $p = 1/7$  is often used (Peterson and Hennessey Jr 1978).

Differentiating Eq. (2.54), we obtain the expression by Huang (1979):

$$p = \frac{z}{u} \cdot \frac{\partial u}{\partial z}. \quad (2.55)$$

This method offers a more complicated approach including also a dependency on the roughness of the surface and the stability using universal functions of the Monin-Obukhov similarity theory (see Sect. 2.2.1). Irvin (1978) proposed the following simple equation:

$$p = \frac{u_*}{u \cdot \kappa} \cdot \varphi_m(\zeta). \quad (2.56)$$

The factor  $u \cdot \kappa \cdot u_*^{-1}$  can be expressed by the integrated form of the universal function given in Sedefian (1980):

$$p = \frac{\varphi_m\left(\frac{\bar{z}}{L}\right)}{\left[ \ln\left(\frac{\bar{z}}{z_0}\right) - \psi_m\left(\frac{\bar{z}}{L}\right) \right]}. \quad (2.57)$$

Huang (1979) used also this form but used the concrete universal functions by Webb (1970) and Dyer (1974) allowing for large roughness elements in contrast with the earlier integration provided by Paulson (1970). For the unstable case, it follows

$$p = \frac{(1 - 16 \frac{\bar{z}}{L})^{-1/4}}{\ln \frac{(\eta-1)(\eta_0+1)}{(\eta+1)(\eta_0-1)} + 2 \tan^{-1} \eta - 2 \tan^{-1} \eta_0} \quad (2.58)$$

$$\eta = \left(1 - 16 \frac{\bar{z}}{L}\right)^{1/4} \quad \eta_0 = \left(1 - 16 \frac{z_0}{L}\right)^{1/4}$$

and for the stable case:

$$p = \frac{1 + 5\frac{z}{L}}{\ln \frac{z}{z_0} + 5\frac{z}{L}}. \quad (2.59)$$

This approach is used in the footprint model by Kormann and Meixner (2001). According to Högström (1988), the coefficients 16 and 5 should be replaced by 19.3 and 6.0.

The use of this method is fraught with difficulties. In the hours before noon, when in the presence of a developing convective boundary layer, the method works well. Later in the afternoon, due to the cooling by longwave upwelling radiation, the layer close to the surface becomes stable while the layers above are still unstable (see Sect. 2.3.2.). Therefore, the stability measured near the surface cannot be applied using the power law. This is because atmospheric stratification sets in first near the surface due to radiative cooling early in the late afternoon and evening while aloft, the upper layers of the atmosphere are still unstable (Foken 2008).

### 2.2.6 Dispersion Profiles

Standard deviations of the three wind components are necessary input parameters of analytical footprint models which are based on a Gaussian dispersion approach. Lagrangian footprint models also need parameterizations of the profiles of standard deviations in the canopy (in the case of tall vegetation) and above.

The similarity between fluxes and variances based on the equation of the turbulent kinetic energy or on analogue equations for sensible heat and other scalars (flux-variance similarity, see Foken 2008). In these equations, the standard deviations of the vertical wind component and the temperature or another scalar are included (Wyngaard and Coté 1971; Foken et al. 1991):

$$\sigma_w = \sqrt{w'^2} \quad \text{and} \quad \sigma_T = \sqrt{T'^2}. \quad (2.60)$$

The normalized standard deviations are also called integral turbulence characteristics (Tillman 1972), because they characterize the atmospheric turbulence over the entire range of turbulence spectra. In the surface layer and in steady-state conditions, these characteristics of the three wind components in the neutral case (Lumley and Panofsky 1964; Panofsky 1984) can be expressed as:

$$\begin{aligned} \sigma_w/u_* &\cong 1.25 \\ \sigma_u/u_* &\cong 2.45 \\ \sigma_v/u_* &\cong 1.9. \end{aligned} \quad (2.61)$$

In the atmospheric surface layer, the turbulence is anisotropic. Therefore the standard deviations of the wind components are different,  $\sigma_w < \sigma_v < \sigma_u$ . For

**Table 2.8** Integral turbulence characteristics for stable and unstable conditions (Foken 2008)

Parameter	$z/L$	$c_1$	$c_2$
$\sigma_w/u_*$	$0 > z/L > -0.032$	1.3	0
	$-0.032 > z/L$	2.0	1/8
$\sigma_u/u_*$	$0 > z/L > -0.032$	2.7	0
	$-0.032 > z/L$	4.15	1/8
$\sigma_T/T_*$	$0.02 < z/L < 1$	1.4	-1/4
	$0.02 > z/L > -0.062$	0.5	-1/2
	$-0.062 > z/L > -1$	1.0	-1/4
	$-1 > z/L$	1.0	-1/3

non-neutral conditions, a large number of parameterizations is given in the literature (Foken 2008). For the wind components, these follow the form

$$\sigma_{u,v,w}/u_* = c_1 \cdot (z/L)^{c_2} \quad (2.62)$$

and for the temperature or other scalars (with a different normalization instead of  $T_*$ )

$$\sigma_T/T_* = c_1 \cdot (z/L)^{c_2}. \quad (2.63)$$

An example of the integral characteristics for unstable (not free convection) and neutral conditions is given in Table 2.8. In the stable case, there are only a few parameterizations available. One can use the above given parameterizations only for the wind components of the unstable case also for the stable case as a first approach.

For the vertical wind component, most studies agree with one another with the parameterization given by Panofsky et al. (1977) is mainly used for a wide range of stratification,  $-1 < z/L < 0$ :

$$\sigma_w/u_* = 1.3 \cdot \left(1 - 2 \cdot \frac{z}{L}\right)^{1/3}. \quad (2.64)$$

The integral turbulence characteristics for temperature and other scalars are in the neutral case due to  $T_* \rightarrow 0$  not well defined. In the unstable range, these turbulence properties are closely coupled to atmospheric stability.

Several authors also found a dependency on the mixed layer height (Panofsky et al. 1977; Peltier et al. 1996; Johansson et al. 2001; Thomas and Foken 2002). This dependency arises mostly in very unstable conditions. Other authors (Yaglom 1979; Tennekes 1982; Högström 1990; Smedman 1991) assumed a dependency on the Coriolis parameter, probably only for neutral conditions to be statistically significant. This was first found by Högström et al. (2002).

For free convective conditions ( $z/L < -1$ ), the scaling parameter is the convective velocity (*Deardorff-velocity*)

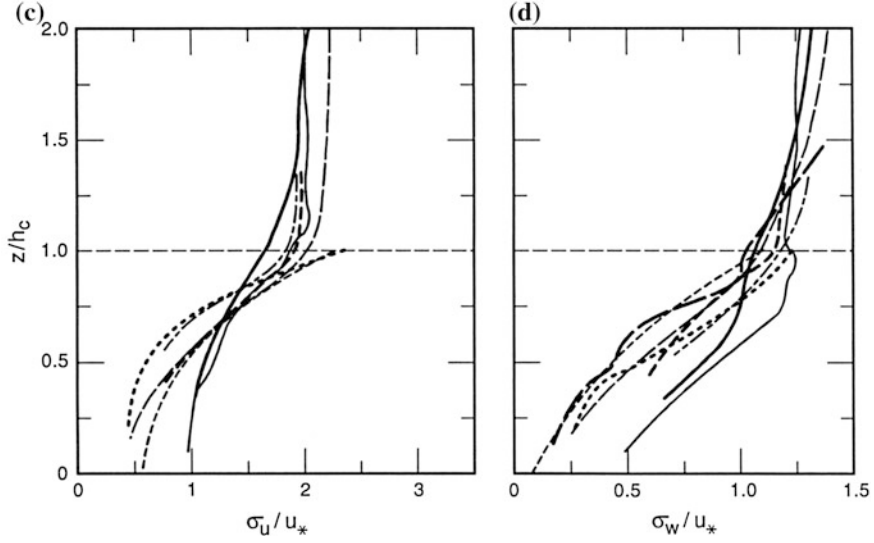


**Fig. 2.9** Profiles of the standard deviation of the horizontal and vertical wind component for wind tunnel, corn and forest measurements by different authors (Kaimal and Finnigan 1994), for legend see Fig. 2.8. (Published with kind permission of © Oxford University Press, 1994. All Rights Reserved)

$$w_* = \left( \frac{g \cdot z_i}{\theta_v} \cdot \overline{\theta'_v w'} \right)^{1/3} \quad (2.65)$$

and partly the mixed layer height  $z_i$  (Garratt 1992). Such parameterizations must take into account the decrease of the characteristics with increasing height and an increase in the entrainment layer. One possible parameterization is given by Sorbjan (1989):

$$\sigma_w / w_* = 1.08 \left( z / z_i \right)^{1/3} \cdot \left( 1 - z / z_i \right)^{1/3} \quad (2.66)$$

$$\sigma_T / T_* = 2 \left( z / z_i \right)^{-2/3} \cdot \left( 1 - z / z_i \right)^{4/3} + 0.94 \left( z / z_i \right)^{4/3} \cdot \left( 1 - z / z_i \right)^{-2/3}. \quad (2.67)$$

The profiles of the integral turbulence characteristics within the canopy are also of special interest in footprint modeling. These profiles are very similar for different types of canopies when normalized with their value in the height of the top of the canopy. This is illustrated in Fig. 2.9.

Inside the canopy, the profiles are strongly dependent on the leaf area index (Shaw et al. 1988). Furthermore, the profiles are also stability dependent (Shaw et al. 1988; Leclerc et al. 1990, 1991) and change with the coupling stage between the atmosphere and the canopy (Göckede et al. 2007). Also, the application of an

**Table 2.9** Coefficients in Eqs. (2.68) and (2.69) for two forested sites

References	$i$	$a_i$	$\alpha_i$	$\beta_i$	$\gamma_i$
Rannik et al. (2003), neutral, for Hyytiälä site (FI-Hyy)	$u$	2.30	1.0	1.0	-0.3
	$v$	1.75	1.0	0.85	-0.2
	$w$	1.25	0.9	1.2	-0.63
Foken et al. (2012), for Waldstein-Weidenbrunnen site (DE-Bay)	$u$	2.01	8.97	1.37	0.29
	$v$	1.60	5.18	1.11	0.34
	$w$	1.13	0.9	1.2	-0.63

analytical second-order closure model used a plant area profile (Massman and Weil 1999) to represent profiles of integral turbulence characteristics comparable with measured data (Göckede et al. 2007).

At a single site, the functional form of these relationships above the canopy is similar to that of measurements above low vegetation. Due to the lack of coupling between the canopy layer flow and the flow above forest canopies, a universal formulation of turbulence profiles is still conspicuously absent. Nevertheless, a site-specific parameterization is required to accurately model the footprint.

For measurements inside the canopy ( $z < h_c$ ), a parameterization was proposed by Rannik et al. (2003)

$$\frac{\sigma_i}{u_*} = a_i \left\{ \exp \left[ -\alpha_i \left( 1 - \frac{z}{h_c} \right)^{\beta_i} \right] (1 - \gamma_i) + \gamma_i \right\} \quad (2.68)$$

$i = u, v, w; \quad z < h_c$

and above the canopy constant values were assumed

$$\frac{\sigma_i}{u_*} = a_i \quad (2.69)$$

$i = u, v, w; \quad z > h_c.$

The values are given in Table 2.9.

### 2.2.7 Relevance of Profile Parameterizations in Footprint Models

Many footprint models use profile functions for the parameterization of surface layer properties and, if the models are not limited to low vegetation, both the roughness sublayer and profile within the canopy must be parameterized. The discussion below deals with the specific parameterizations and differences between models based on their relevance (Chap. 3). Most footprint models use Monin-Obukhov similarity theory only with minor differences (Table 2.10)

**Table 2.10** The use of surface layer parameterization for the stability influence in the widely distributed footprint models, “*italic*” not according the recently accepted modifications of the universal functions according to Högström (1988)

Footprint model	Use of	Remarks
Gash (1986)		Neutral
Schuepp et al. (1990), Horst and Weil (1992, 1994), Hsieh et al. (2000), Hsieh and Katul (2009)	Monin-Obukhov similarity theory	<i>Universal function by Dyer (1974), but <math>\kappa = 0.4</math></i>
Leclerc and Thurtell (1990)	Monin-Obukhov similarity theory	<i>Universal function by Dyer (1974) for unstable and by Businger et al. (1971) for stable stratification, but <math>\kappa = 0.4</math></i>
Schmid (1994, 1997)	Probably like Horst and Weil (1992; 1994)	
Leclerc et al. (1997)	Monin-Obukhov similarity theory	<i>Universal function by Businger et al. (1971), but <math>\kappa = 0.4</math></i>
Kaharabata et al. (1997)	Monin-Obukhov similarity theory	<i>Universal function by Businger et al. (1971), but <math>\kappa = 0.4</math></i>
Haenel and Grünhage (1999)	Monin-Obukhov similarity theory	<i>Universal function by Dyer (1974)</i>
Rannik et al. (2000, 2003)	Monin-Obukhov similarity theory, roughness sublayer	Universal function by Businger et al. (1971) in the re-evaluated form by Högström (1988)
Kormann and Meixner (2001)	Combination of power law and Monin-Obukhov similarity theory according to Huang (1979)	<i>Universal function by Webb (1970) and Dyer (1974)</i>
Kljun et al. (2002)	Monin-Obukhov similarity theory and convective boundary layer	See Rotach et al. (1996): universal function by Businger et al. (1971) in the re-evaluated form by Högström (1988)

between each other. Furthermore, most footprint models require a parameterization of the standard deviations of the wind components. In Lagrangian models, this parameterization is mainly those of vertical wind components, while, in the two-dimensional analytical case, the parameterization must include those of the lateral wind component (Table 2.11).

## 2.3 Internal Boundary Layers

The above given parameterizations of the atmospheric turbulence are based on the assumption of horizontal homogeneity. Landscapes are composed of a mosaic of typically heterogeneous surfaces with a change in surface characteristics within the



**Table 2.11** The use of surface layer parameterization of the standard deviation of the wind components in the widely distributed footprint models

Footprint model	Use of	Remarks
Leclerc and Thurtell (1990)	Similar to Lumley and Panofsky (1964) in the neutral and stable case and Panofsky et al. (1977) and Hicks (1981) in the unstable case	Vertical wind component
Horst and Weil (1992, 1994)	Panofsky et al. (1977)	Vertical wind component
Hsieh et al. (2000) and Hsieh and Katul (2009)	See Leclerc and Thurtell (1990)	Vertical wind component
Rannik et al. (2000, 2003)	Similar to Panofsky et al. (1977)	

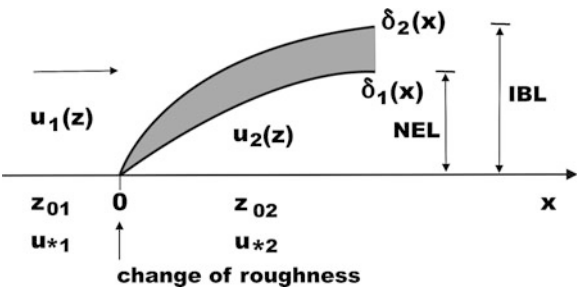


**Fig. 2.10** Schematic structure of the internal boundary layer at a sudden change of the surface roughness according with the new equilibrium layer (NEL), the internal boundary layer (IBL), the fetch  $x$ , and the discontinuity layer between both according to the findings by Rao et al. (1974) from Foken (2008)

first 100 m. The wind profile develops depending on surface roughness, temperature profile-dependent on the surface temperature, etc. on the downwind site of such changes in the surface characteristics. Due to the horizontal wind field, the different profiles are shifted downwind. Therefore, internal boundary layers are significantly developed close to the surface. These arise in the presence of horizontal advection over discontinuities of surface properties (roughness, thermal properties, etc.). Overviews are given by Stull (1988), Garratt (1990, 1992) and Savelyev and Taylor (2001, 2005).

The internal boundary layer is a disturbed layer, which can be divided into different layers (Fig. 2.10). The layer below the discontinuity layer is called new equilibrium layer (NEL). Their properties come from the new surface. Above that layer (internal boundary layer, IBL), the layer is influenced by the surface on the upwind site. Above the new equilibrium layer, the discontinuity layer is not a sharp line but rather covers a range. For large fetches, the differences between both sides of an internal boundary layer decrease.

The concept of the internal boundary layer was used by Schmid and Oke (1990) to define the outer dimensions of the source area within the new equilibrium layer.

Typical fetch requirements for measurement levels located within the presence of internal boundary layers scale with the scale of footprint areas (Horst 2000). Nevertheless, the footprint concept provides an essential contribution to measurement sites, since most footprint models are not able to determine the effect of roughness changes. Some progress was made by Luhar and Rao (1994) and further on by Klaassen and Sogatchev (2006) for footprints at a forest edge and by Markkanen et al. (2010) for thermal heterogeneous surfaces. The practical application of the internal boundary-layer concept is discussed in Sect. 8.1.

### 2.3.1 Mechanical Internal Boundary Layer

The development of a mechanical internal boundary layer is caused by mechanical inhomogeneities both upwind and downwind (roughness length). In the simplest case, the height of an internal boundary layer can be determined by extrapolating the wind profiles above and within the internal boundary layer (Elliott 1958; Raabe 1983):

$$u_1(\delta) = u_2(\delta). \quad (2.70)$$

This method has the disadvantage that the point of intersection may be above the internal boundary layer or within the new equilibrium layer. More successful is the assumption that the undisturbed wind profile can be well fixed below and above the internal boundary layer and the height is between the upper and lower point of disturbance:

$$\delta = \frac{\delta_1 + \delta_2}{2}. \quad (2.71)$$

For practical reasons, it can be useful to use the lower level of the layer of disturbances as the height of the internal boundary layer,  $\delta = \delta_l$ , because the new equilibrium layer can be assumed to be as undisturbed above the new surface (Rao et al. 1974) enabling the experimentalist to make measurements within that layer that reflect the properties of the surface beneath.

The mechanical internal boundary layer occurs for the flow from rough to smooth as well as from smooth to rough. Since different wind gradients differ between above smooth and rough surfaces, there is a characteristic development of internal boundary layers (Fig. 2.11).

The dependency of the height of an internal boundary layer on the fetch  $x$  was found in hydrodynamical investigations and is given by a 4/5-exponential law (Shir 1972; Garratt 1990; Savelyev and Taylor 2001):

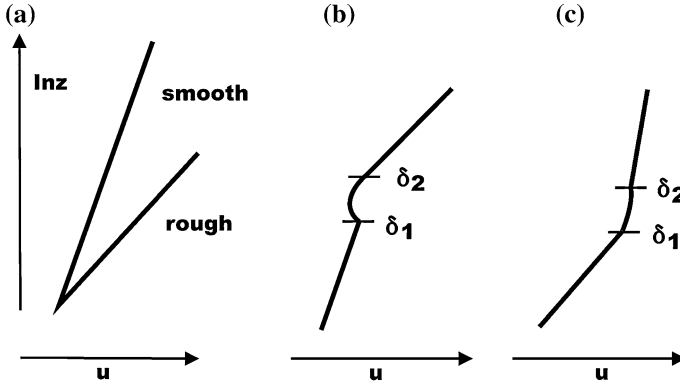


**Fig. 2.11** The schematic wind profile at an internal boundary layer for neutral stratification: **a** typical profile for rough and smooth surfaces, **b** Change of the surface roughness from rough to smooth, **c** Change of the surface roughness from smooth to rough (Foken 2008)

**Table 2.12** Experimental results for the coefficients in Eq. (2.73) to depend the height of the internal boundary layer (new equilibrium layer according to Rao et al. 1974), for more data see Savelyev and Taylor (2005)

Author	a	b	Conditions
Bradley (1968), Shir (1972)	0.11	0.8	$z_{01}/z_{02} = 125$ and 0.08 artificial roughness
Antonia and Luxton (1971, 1972)	0.28 0.04	0.79 0.43	$x \leq 10$ m, rough–smooth $x \leq 10$ m, smooth–rough wind tunnel
Raabe (1983)	$0.30 \pm 0.05$	$0.50 \pm 0.05$	Beach, on- and off-shore winds, $5 \text{ m} < x < 1,000 \text{ m}$

$$\delta = f_1 \left( z_{01}/z_{02} \right) \cdot x^{4/5 + f_2(z_{01}/z_{02})}. \quad (2.72)$$

A lot of experiments were done to verify this equation. Because of the large scatter in experimental results, most of the authors assume a simplified dependency

$$\delta = a \cdot x^b \quad (2.73)$$

for which some data are given in Table 2.12.

The height of the internal boundary layer normalized by the upwind roughness length was found to be higher for smooth to rough transition than for rough to smooth transition according to model calculations (Garratt 1990; Savelyev and Taylor 2001) and also the internal boundary layer is higher in the unstable case than in the stable case (Savelyev and Taylor 2005). But in the case of experimental

data, no significant differences in the height of the internal boundary layer could be found due to the large scatter in the experimental data (Jegede and Foken 1999). Therefore, simple parameterizations of the internal boundary layer or equilibrium layer height according to Eq. (2.73) with the coefficients by Raabe (1983) are a good approach.

Large fetch requirements of internal boundary layers have constituted the basis of micrometeorological measurements for decades. Micrometeorological measurements were typically done at height/fetch ratios of 1/100 of undisturbed fetch. This requirement for the measuring height  $z_m = 100x$  gives similar results as Eq. (2.73). Leclerc and Thurtell (1990) found that the 1:100 ratio used by micrometeorologists agrees with footprint calculations for short crop canopies in unstable conditions.

### 2.3.2 Thermal Internal Boundary Layer

In analogy to the mechanical internal boundary layer formed by a sudden change in surface roughness, a thermal internal boundary layer develops as a result of a change in surface temperature due to different land-use characteristics. Furthermore, other surface characteristics like different surface moisture or gas exchange conditions can lead to a scalar internal boundary layer. Few if any experimental results are available on the subject since this layer is typically combined with the mechanical internal boundary layer.

The height of the thermal internal boundary layer is given by Raynor et al. (1975):

$$\delta_T = c \left( \frac{u_*}{u} \right) \left[ \frac{x (\theta_1 - \theta_2)}{|\partial T / \partial z|} \right]^{1/2}. \quad (2.74)$$

The temperature gradient is measured on the upwind side or above the internal boundary layer, all other parameters in the reference level. The coefficient  $c$  depends on the reference level and is in the order of 1 (Arya 2001). Obviously, such parameterizations are similarly robust as in Eq. (2.73) for the mechanical internal boundary layer.

A special case is the thermal internal boundary layer during the afternoon mainly due to the “oasis effect” (Stull 1988). Shortly after noon above an evaporating surface, the temperature near the surface decreases and the stratification becomes stable. The height of the deflection point between stable stratification near the surface and the unstable conditions in the higher layers grows over time. This inversion layer close to the surface is also called a thermal internal boundary layer. Below the inversion, the sensible heat flux is downward and above upward. The height increases up to 50–100 m after sunset and is then identical with the

stable boundary layer (see [Sect. 3.1](#)). According to this finding, the thermal internal boundary layer exists over a period of several hours at typical micrometeorological levels. Also in the early morning, this effect can be found, but with a much shorter duration, i.e. of the order of minutes. The problem is of particular relevance when the stability near the surface is used e.g. to determine the power law in the lower atmospheric boundary layer. The consequence on footprint models in the afternoon has not yet been investigated.

### 2.3.3 Blending Height Concept

According to the structure of internal boundary layers, it can be assumed that the internal boundary layers can only develop up to a certain level. The layers merge with one another far away from the change in surface roughness. Above this height, an area-averaged flux can be assumed. That means the properties near the surface fade (Taylor 1987). This idea is the basis of the so-called blending height concept according to Mason (1988) and its updated formulations by Claussen (1991) and Claussen and Walmsley (1994). The blending height is assumed to be at heights ranging between approximately 30–100 m with a close dependence on the magnitude of the underlying surface roughness and atmospheric conditions. The concept considers especially larger scale changes in surface roughness with characteristically horizontal distances of  $L_x > 1$  km. The blending height  $l_b$  can be estimated as (Mahrt 1996)

$$l_b = 2 \left( \frac{u_*}{u} \right)^2 L_x \approx 2 \left( \frac{\sigma_w}{u} \right)^2 L_x \quad (2.75)$$

or as a simple approximation  $l_b = L_x / 200$ .

The blending height concept has a large practical evidence for area averaging in numerical models (see [Sect. 2.4](#)), because it can be assumed for the model level in the height of approximately the blending height the fluxes above an heterogeneous surface are area averaged (Claussen 1995).

From the experimental standpoint, this concept is controversial. In an atmospheric boundary layer, conditions of free convection exist for  $z/L < -1$ , and for example for  $z/L = -0.1$  at 2 m height, free convection starts already above 20 m (Eigenmann et al. 2009). According to Andreas and Cash (1999), the conditions for free convection are given for  $\delta/L < -1$  in a growing internal boundary layer. This is a level where internal boundaries can be easily detected. The conditions of single surfaces can be also detected by aircraft measurements in the whole boundary layer if the single areas are large enough that convection can be developed. This is the case for horizontal extensions larger 200 m (Shen and Leclerc 1994). The convection areas can be typically found several hundreds of meters on the downwind side of the roughness change due to the development of internal boundary layers.

## 2.4 Modeling Concepts

In the following chapter, modeling concepts used to describe the family of footprint models will be presented. The specific application of these model types is presented in [Chap. 3](#).

### 2.4.1 Diffusion Model

The diffusion model based on Pasquill (1972) was the most widely used type of models used for footprint modelling as most analytical models applied this method. The simplest models often used in air pollution applications are Gaussian plume models (Pasquill 1972; Pasquill and Smith 1983; Blackadar 1997; Arya 1999). The dispersion of air pollution in a three-dimensional volume can be described with probability density functions for the distribution of pollutants or particles in the three directions  $F(x)$ ,  $G(y)$ , and  $H(z)$ . The three-dimensional distribution becomes, according to the continuity principle

$$\int_{-\infty}^{\infty} \int_{-\infty}^{\infty} \int_{-\infty}^{\infty} F(x)G(y)H(z) dx dy dz = 1. \quad (2.76)$$

For a point source with constant emission rate  $Qdt$  and constant horizontal wind velocity, the distribution density function is:

$$F(x) = \frac{1}{\bar{u} dt}. \quad (2.77)$$

For the transverse horizontal and vertical distributions, the Gaussian distribution functions are used:

$$G(y) = \frac{1}{\sqrt{2\pi} \sigma_y} \exp\left(-\frac{y^2}{2\sigma_y^2}\right) \quad (2.78)$$

$$H(z) = \frac{1}{\sqrt{2\pi} \sigma_z} \exp\left(-\frac{z^2}{2\sigma_z^2}\right) \quad (2.79)$$

where  $\sigma_y$  and  $\sigma_z$  are the standard deviations of the lateral and vertical wind component.

The concentration distribution can be also calculated using Fick's diffusion law:

$$\frac{\partial \chi}{\partial t} + \bar{u} \frac{\partial \chi}{\partial x} = \frac{\partial}{\partial x} \left( K_x \frac{\partial \chi}{\partial x} \right) + \frac{\partial}{\partial y} \left( K_y \frac{\partial \chi}{\partial y} \right) + \frac{\partial}{\partial z} \left( K_z \frac{\partial \chi}{\partial z} \right). \quad (2.80)$$

The parameterization of the diffusion coefficients is made with error functions:

$$\sigma_u^2 = 2 K_x t \quad \sigma_v^2 = 2 K_y t \quad \sigma_w^2 = 2 K_z t. \quad (2.81)$$

The concentration distribution for a constant source strength  $Q$  and the mean horizontal wind speed  $\bar{u}$  in the  $x$ -direction is given by

$$\chi(x, y, z) = \frac{Q}{2 \pi \bar{u} \sigma_v \sigma_w} \exp \left( -\frac{y^2}{2 \sigma_v^2} - \frac{z^2}{2 \sigma_w^2} \right). \quad (2.82)$$

In the absence of meteorological data, the standard deviations of the wind components can be parameterized using the micrometeorological approach described in Sect. 2.2.6. Gryning et al. (1987) use a plume crosswind dispersion based on Draxler (1976), which includes the Lagrangian time scale (see below) for crosswind dispersion.

The most widely applied footprint models are based on the analytical solution of the vertical diffusion by van Ulden (1978) and Gryning et al. (1983, 1987) determined solutions for Eq. (2.82) for individual atmospheric scenarios. For the vertical diffusion, it follows

$$\frac{\chi_z(x, z)}{Q} = \frac{A}{\bar{z}(x)} \exp \left[ -\left( \frac{B \cdot z}{\bar{z}} \right)^r \right] \quad (2.83)$$

and for crosswind diffusion

$$\frac{\chi_y(x, y)}{Q} = \frac{A}{\bar{z}(x) \bar{u}} \exp \left[ -\left( \frac{B \cdot y}{\bar{z}} \right)^r \right] \quad (2.84)$$

where  $A = r \cdot \Gamma(2/r)/\Gamma^2(1/r)$  and  $B = \Gamma(2/r)/\Gamma(1/r)$  are functions of the shape parameter  $r$  and  $\Gamma$  is the gamma function and  $\bar{z}$  is the mean height of the plume. In some cases, a Gaussian distribution is commonly used to include the diffusion in the lateral direction:

$$\frac{\chi_y(x, y)}{Q} = \frac{1}{\sqrt{2\pi} \cdot \sigma_v} \exp \left[ -\frac{1}{2} \left( \frac{y}{\sigma_v} \right)^2 \right] \quad (2.85)$$

where  $A$  and  $B$  are functions of the exponent (shape parameter)  $r$ . Gryning et al. (1983) provided an approximate formula for  $r$  in terms of the mass-weighted mean plume height,  $\bar{z}(x)$  and stability.  $\bar{u}$  is the mass-weighted mean plume velocity. Although van Ulden's solution is analytical, it is implicitly in  $x$  by

**Table 2.13** The use of diffusion model parameterizations in the widely distributed footprint models

Footprint model	Use of
Gash (1986)	Pasquill (1961)
Schuepp et al. (1990),	Gash (1986)
Horst and Weil (1992, 1994)	van Ulden (1978), Horst (1979)
Schmid (1994, 1997)	van Ulden (1978), Gryning et al. (1987)
Haenel and Grünhage (1999)	van Ulden (1978), Horst (1999)
Kormann and Meixner (2001)	van Ulden (1978), Horst and Weil (1992)

$$\bar{z}(x) = \frac{\int_0^{\infty} z \chi_y(x, y) dz}{\int_0^{\infty} \chi_y(x, y) dz}. \quad (2.86)$$

Using  $K$ -theory, van Ulden (1978) expressed the evolution of the centroid of the plume

$$\frac{d\bar{z}}{dx} = \frac{K(p\bar{z})}{\bar{u}(p\bar{z})p\bar{z}} \quad (2.87)$$

where  $K$  is the eddy diffusivity, and  $p$  is a weak function of  $x$ . The wind profile above the canopy is given by the logarithmic wind profile in Eq. (2.39), while the mean wind profile inside a canopy is given in Eq. (2.44).

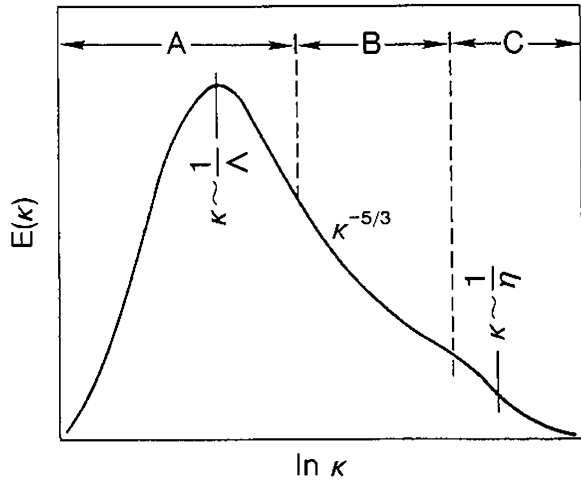
An overview of the different uses of diffusion model parameterizations in analytical footprint models is given in Table 2.13.

### 2.4.2 Lagrangian Model

The spectrum of atmospheric turbulence scales (Frisch 1995) for state parameters and fluxes in the range of micrometeorological processes (periods lower than approx. 30 minutes depending on the site properties, altitude, etc.) is divided into three regions. The range of energy transfer from the mean motion into turbulent flow is characterized by the integral turbulent length scale  $\Lambda$ , which is approx.  $10^1$ – $5 \cdot 10^2$  m (Kaimal and Finnigan 1994). The typical range of frequencies is  $f \sim 10^{-4}$  Hz. High frequencies follow the inertial sub range with isotropic turbulence. This range follows Kolmogorov's law (Kolmogorov 1941a, b) with a defined decrease in energy density with increasing frequency in a manner proportional to  $f^{-5/3}$ . At higher frequencies ( $f \sim 10$ – $30$  Hz), eddies disappear through viscous dissipation  $\varepsilon$ . The scale is the Kolmogorov's micro-scale of about  $10^{-3}$  m:



**Fig. 2.12** Schematic illustration of the turbulence spectra with the range of energy production (a), Energy dissipation (c) and the inertial subrange (b) depending on the wave number  $\kappa$  (Kaimal and Finnigan 1994, Published with kind permission of © Oxford University Press, 1994. All Rights Reserved)



$$\eta = \left( \frac{v^3}{\varepsilon} \right)^{1/4} \quad (2.88)$$

The three ranges in the turbulence spectra in micrometeorology are illustrated in Fig. 2.12 as a function of wave length. The spectral peak corresponds to an integral turbulent length scale (exact:  $\kappa = \pi/\Lambda$ ,  $\Lambda$ : Eulerian length scale). This length scale can be determined for wind components and scalars. According to Taylor's hypothesis on frozen turbulence (Taylor 1923, 1938), for which the relation

$$\kappa = 2\pi \cdot f / \bar{u} \quad (2.89)$$

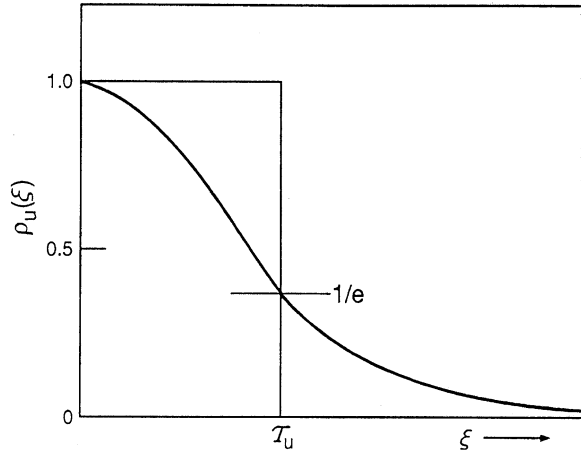
is valid, this length scale can be combined with the integral turbulent time scale using the mean wind velocity.

The Lagrangian integral time scale  $\tau$  can be determined from the autocorrelation function  $\rho$  (Monin and Yaglom 1973, 1975; Schlichting and Gersten 2003; Wyngaard 2010). Because the autocorrelation function is usually an exponential function, the integral time scale of  $\xi$  is  $\rho(\xi) = 1/e \sim 0.37$ . This is illustrated in Fig. 2.13. For the horizontal length scale follows with the horizontal wind velocity:

$$\Lambda_u = \bar{u} \cdot \tau_u = \bar{u} \int_0^\infty \rho_u(\xi) d\xi = \bar{u} \int_0^\infty \frac{\overline{u'(t) u'(t + \xi)}}{\sigma_u^2} d\xi. \quad (2.90)$$

The transport of a conserved passive scalar be it of carbon dioxide, water vapor or the likes is predicated on the state of the atmosphere. The atmosphere near the

**Fig. 2.13** Autocorrelation function and its dependency on the integral time scale. The value  $1/e$  is a good approximation for which the square of the rectangle is identical with the square below the exponential graph (Kaimal and Finnigan 1994, Published with kind permission of © Oxford University Press, 1994. All Rights Reserved)



ground is characterized by vertical inhomogeneity in the flow, i.e.  $\tau = \tau(z)$ , the Lagrangian time scale of the turbulence, is thought to be a function of height. Earlier, seminal studies of Wilson et al. (1981) have found this value to  $\tau \sim 0.5z$  in the neutral atmospheric surface layer above a smooth surface. The Lagrangian timescale plays an important role in Lagrangian modeling (Koeltzsch 1999).

The atmospheric surface layer is also generally the layer of air where anisotropy ( $\sigma_u > \sigma_v > \sigma_w$ ) is significant,  $\sigma_{u_i} = \sigma_{u_i}(z)$ , where  $\sigma_{u_i}$  is the turbulence velocity scale in dimensions i.e. the streamwise, crosswind, and vertical directions increases with distance from the surface in the surface layer (see Sect. 2.2.6). It is customarily assumed that the Eulerian and the Lagrangian turbulent velocity scales of the turbulence are equivalent, thus greatly simplifying our prescription of input variables. In the neutral case, Wilson et al. (1982) found for the vertical and horizontal wind velocity, the time scales can be defined as

$$\tau_w = \frac{0.1 z}{\sigma_w(z)}, \quad \tau_u \equiv \tau_L = \frac{0.5 z}{\sigma_w(z)}, \quad (2.91)$$

which were used by Leclerc and Thurtell (1990) in the original Lagrangian footprint model. In the neutral atmospheric surface layer,  $\sigma_w(z)$  in the Lagrangian timescale can also be replaced by  $1.25u_*$  according to Eq. (2.61).

The integral time scale used in Lagrangian footprint models is given in Table 2.14.

The trajectory of the fluid element is given as

$$du_i = u_i dt \quad (2.92)$$

where  $u_i$  is the instantaneous Lagrangian velocity in the  $x_i$  direction and where  $dt$  is the instantaneous time increment, typically taken to be generally  $0.1 \tau$ :

**Table 2.14** The use of surface layer parameterization for the Lagrangian integral time scale in the widely distributed footprint models, “*italic*” not according the present state

Footprint model	Use of	Remarks
Leclerc and Thurtell (1990)	$\tau(z) = \frac{0.5 z}{\sigma_w(z)}$	Wilson et al. (1982)
Baldocchi (1997)	$\tau = \frac{0.3 h_c}{u_*}$	<i>No height dependence</i>
Rannik et al. (2000, 2003)	$\tau = \frac{2\sigma_w^2}{C_0 \epsilon}$	$C_0 = 4$ (Kolmogorov constant)

$$u_i = a_i(x_i, t)dt + b_i(x_i, t)r. \quad (2.93)$$

With the first term representing the ‘memory’ term and the second term the ‘random’ term. Both  $a_i$  and  $b_i$  are a function of position, time and velocity while  $r$  is a random process with Gaussian statistics, exhibiting a mean of zero and a variance of 1. It is the respective magnitude of each of the coefficients that dictate the relative weight of the ‘memory’ term and that of the ‘random’ term. In inhomogeneous turbulence as are the cases treated here, an additional term must be added. The characteristics of the latter but a drift term is generally sufficient to treat the diffusion near a simple surface in the atmospheric surface layer. That original method has often yielded to the generalized method used by Thomson (1987) to deal with inhomogeneous turbulence.

An asset of Lagrangian stochastic models over analytical solutions lies in their applicability to model the dispersion from a very close range (near field), a subject of particular importance inside vegetation i.e. the region of sources and sinks. Lagrangian simulations intrinsically account for the characteristics of diffusion both in the near-field and in the far field as particles travel away from their source; this key feature allows for a proper description of the physics within vegetation (Denmead and Bradley 1985; Thurtell 1988).

### 2.4.3 Higher-Order Closure Model

Over the last decade, also classical numerical models based on the Navier-Stokes equations have also been used in modeling atmospheric footprints. The transformation of streamwise flow components into the equations of motion to the equation for turbulent flow is necessary. This leads to a system of differential equations with more unknown parameters than equations. To solve the system of equations, assumptions have to be made to calculate the unknown parameters. This is often referred to as closure techniques.

The order of the closure refers to the highest order of the parameters that must be calculated with the prognostic equations. Therefore, the moments of the next higher order must be determined (Stull 1988). A first-order closure generally use either the  $K$ -closure approach or stability functions linked to Monin-Obukhov similarity theory. To calculate state variables like the wind velocity or

temperature, the  $K$ -approach must be applied to determine fluxes according to Eqs. (2.24)–(2.26). With a second-order closure, turbulent fluxes can be determined using the prognostic equation, but a parameterization for the triple correlation is necessary. A 1.5 order closure uses the equation of the turbulent kinetic energy (Stull 1988) to determine variance terms, see Sect. 2.2.6.

The benefit of closure techniques larger than the first-order closure allows the modeling of counter gradients, a frequent occurrence inside canopies (Denmead and Bradley 1985). In the case of counter gradient diffusion, the direction of the flux does not follow the direction of the gradient due to possible exchange by coherent structures, while the proportionality between flux and gradient is given for the  $K$ -approach (1st order closure). The models by Sogachev et al. (2002, 2008), Sogachev and Panferov (2006), and Sogachev and Leclerc (2011) are of 1.5 order closure and by Hsieh and Katul (2009), Hsieh et al. (2000), and Luhar and Rao (1994) of 2nd order closure.

#### 2.4.4 Large-Eddy Simulation Model

This Large-Eddy Simulation (LES) method, applied for the first time to the atmosphere by Deardorff (1972) and Moeng and Wyngaard (1988), is considered the *ne plus ultra* approach for complex flows not otherwise within the realm of most models; LES can also incorporate pressure gradients and other challenging flow/surface scenarios conferring it a definite advantage.

The LES approach is based on the fact that most of the flux is contained in the large eddies, which are directly resolved. Therefore, a parameterization is necessary to account for the contribution of smaller eddies to fluxes. This method provides a high level of realism of the flow despite complex boundary conditions. This powerful type of simulations has been used extensively in atmospheric flow modeling and in particular in convective boundary layers (Mason 1989).

The LES computes the three-dimensional, time-dependent turbulence motions, and only parameterizes the subgrid-scale motions (SGS). Using the Navier-Stokes equations, LES resolves the large eddies with scales equal to or greater than twice the grid size, while parameterizing SGS processes.

The LES approach is free of the drawback of prescribing a turbulence field, hence the importance of initial and boundary conditions. Typically, LES determines the three-dimensional velocity field, pressure, and turbulent kinetic energy. The LES can also contain a set of cloud microphysical and thermodynamic equations and can predict the temperature and mixing ratios. It can also simulate the turbulent transport of moisture, carbon dioxide, and pollutants.

The first seminal study using the LES to model the turbulence inside a forest canopy was performed by Shaw and Schumann (1992). That study revealed the feasibility of using the LES to model correctly the three-dimensional structure of the turbulence in the canopy layer. In the absence of experimental data, LES is often a substitute, providing a realistic turbulence structure. Canopy LES simulations were

made for homogeneous canopy flows (Patton et al. 2001; Shaw and Patton 2003; Yue et al. 2007; Mao et al. 2008; Shen and Leclerc 1997; Su et al. 1998) and recently to the canopy layer near the edge (Dupont and Brunet 2009).

There are several parameterizations available in treating the sub-grid scales. One of the most widely used simulations is that originally developed by Moeng (1984) and Moeng and Wyngaard (1988) and later adapted for flux footprint applications by Leclerc et al. (1997) and Mao et al. (2008). Often, the in canopy SGS are parameterized using the 1.5 order of closure scheme. Sullivan et al. (2003) have discussed and proposed realistic closure schemes.

Some LES also include a terrain-following coordinate system. A spatial cross-average and temporal average is most often applied to the simulated 'data' once the simulation has reached quasi steady-state equilibrium. Typical boundary conditions are periodic with a rigid lid applied to the top of the domain so that waves are absorbed and reflection from the upper portion of the domain is decreased. The LES is computationally very expensive and limited by the number of grid points in flow simulations. As computers' performance and speed keep going up, this becomes less and less of an issue though still of significance when footprint modeling in moderately stable conditions is required.

Despite the many advantages of the present method, moderately stable boundary layers remain the Achilles' heel of the LES, with errors due to an imperfect SGS becoming more pronounced in these stable conditions since the characteristic eddy size is notably smaller.

The LES technique is generally prized amongst other numerical modeling approaches in part because, as is the case for a canopy layer, they have reproduced key features of the canopy turbulence structure such as vertically distributed shear levels, high turbulence intensities changing rapidly with depth inside the canopy layer, scalar microfronts and inflection point near treetop in the velocity profile (Su and Leclerc 1998; Su et al. 1998; Fitzmaurice et al. 2004; Watanabe 2004; Yue et al. 2007; Mao et al. 2008).

The LES technique is applied for footprint modeling either in the way that the LES model produces the necessary input parameters e.g. for a Lagrangian footprint model (Leclerc et al. 1997) or by embedding an Lagrangian footprint model directly into the LES model (Steinfeld et al. 2008). The footprint application of LES models is still an ongoing issue.

## 2.5 Averaging Surface Characteristics

Most footprint models are based on atmospheric transport patterns over regions with spatially uniform flux sources and surface characteristics (e.g. roughness length, leaf area index, or surface moisture). Lagrangian backward models (Kljun et al. 2002), Large-Eddy Simulation (e.g. Steinfeld et al. 2008) and higher-order closure models (e.g. Sogachev and Lloyd 2004) provide complex footprint descriptions over heterogeneous surfaces. Simpler footprint models needs the

averaging of the surface characteristics of a heterogeneous surface to determine averaged input parameters.

The net impact of spatially heterogeneous surface characteristics on atmospheric transport, and therefore on footprint computations is governed by highly non-linear processes. Despite the above, many approaches that sacrifice complex physics are available for the sake of mathematical simplicity. The simplest approach available, called the parameter aggregation, linearly averages parameters such as the aerodynamic roughness length over an area characterized by surface parcels of distinct properties

$$\bar{z}_0 = \frac{1}{N} \sum_{i=1}^N z_{0i}. \quad (2.94)$$

Parameter aggregation is easy to apply and commonly used in footprint studies. This is however achieved at the expense of a significant over simplification of the underlying physics. The error of such averaging can be considerable (Stull and Santos 2000). For example, in the case of a heterogeneous landscape composed of equal parts of water ( $z_0 = 0.001$  m) and of forest ( $z_0 = 1.0$  m), the linearly averaged roughness length would suggest shrub land ( $z_0 = 0.5$  m); however, the flow characteristics over shrubs differ significantly from those over a forested area with lakes.

The reason for the failure of the parameter aggregation is the fact that the interaction of the atmosphere with the underlying surface takes parties intertwined with fluxes such as the momentum flux

$$\tau = \rho \cdot u_*^2 = \frac{\rho}{N} \cdot \sum_{i=1}^N \left( \frac{\kappa \cdot u_i(z)}{\ln z - \ln z_{0i}} \right)^2. \quad (2.95)$$

The relationship between surface characteristics (e.g. roughness length) and resulting fluxes (e.g. momentum flux) is non-linear. Therefore, averaged surface parameters lead to a construction of a regional flux that differs from that created using a superposition of fluxes from the individual patches. Accordingly, these fluxes must be averaged (flux aggregation) to yield more realistic results. Besides the momentum flux, also the stability (momentum and sensible heat flux) and the evaporation (latent heat flux) must be averaged for special applications (Chap. 6). Due to the involvement of additional flux equations and their interdependencies, it is evident that the flux aggregation is complex than parameter aggregation.

### 2.5.1 Averaging Using Effective Parameters

A common approach to arrive at spatially averaged parameter sets that produce representative area-averaged fluxes without the use of complex algorithms consists

in selecting effective parameters. A well-known example is that of the ‘effective roughness lengths’ presented by Fiedler and Panofsky (1972). These effective roughness lengths are not describing the roughness of a particular underlying surface per se, but instead focus on the effect on momentum fluxes on the landscape scale (flat terrain: 0.42 m; low hills: 0.99 m; high mountains: 1.42 m). Generally speaking, the determination of the effective roughness length needs the normalization with the friction velocity inherent to a particular area (Taylor 1987; Schmid and Bünzli 1995a, b; Mahrt 1996; Hasager and Jensen 1999) in the following form:

$$z_{0eff} = \frac{\overline{u_* \cdot \ln z_0}}{\overline{u_*}} \quad (2.96)$$

Such a simple averaging method is helpful for countless practical applications, such as the micrometeorological characterization of the boundary layer above settlement areas (Grimmond et al. 1998).

A more empirical form for the determination of an effective roughness length was presented in the European Wind Atlas (Troen and Peterson 1989). The authors classified only four types (0–3) of the surface roughness (water, flat meadows, landscape with bushes, forest), each of which are assigned a basic roughness length. To include subgrid-scale heterogeneities, the model area is divided up into quarters, each of which are assigned individualist own land-cover class. In Table 2.15 the different portions of the roughness classes (water, flat meadows, landscape with bushes, forest) to the entire area are given. Unfortunately no algorithm is available or published. The effective roughness length is an “empirical” function of the contribution of each surface area to the whole area. Göckede et al. (2004) used this concept to determine an effective roughness length for each grid cell in a heterogeneous landscape. The authors assumed that a simple parameter averaging of these effective values was sufficient to subsequently average the roughness length of all grid cells within the footprint area.

### 2.5.2 Flux-Averaging Models in Inhomogeneous Terrain

The simplest form of a flux aggregation approach is the tile approach, where land cover characteristics within a grid cell accumulate (Fig. 2.14a) according to the proportional use of each land-use type. To arrive at representative averaged parameters, fluxes must be determined for each land use type, and averaged afterwards (Beyrich et al. 2006). However, this method neglects the interaction between the different grid cells, e.g. flow transitions from smooth to rough surfaces or vice versa, local circulation or large water bodies, which can influence the flux systematically. Both experimental (Panin et al. 1996; Klaassen et al. 2002; Klaassen and Sogatchev 2006) and numerical studies (Schmid and Bünzli 1995a;

**Table 2.15** Averaging schema of the roughness length in the European Wind Atlas (Troen and Peterson 1989) used to generate a “flux-averaged” effective roughness length

Type	Water (%)	Flat meadow (%)	Landscape with bushes (%)	Forest (%)	Effective roughness length (m)
$z_0$ (m)	0.0002	0.03	0.1	0.4	
	75	25			0.001
	75		25		0.002
	75			25	0.003
	50	50			0.004
	50	25	25		0.006
	50	25		25	0.010
	50		50		0.009
	50		25	25	0.015
	50			50	0.025
	25	75			0.011
	25	50	25		0.017
	25	50		25	0.027
	25	25	50		0.024
	25	25	25	25	0.038
	25	25		50	0.059
	25		75		0.033
	25		50	25	0.052
	25		25	50	0.079
	25			75	0.117
		75	25		0.042
		75		25	0.064
		50	50		0.056
		50	25	25	0.086
		50		50	0.127
		25	75		0.077
		25	50	25	0.113
		25	25	50	0.163
		25		75	0.232
			75	25	0.146
			50	50	0.209
			25	75	0.292

Friedrich et al. 2000; Sogachev et al. 2008) found that in a heterogeneous landscape, significantly higher fluxes are found close to such roughness changes.

This problem can be circumvented using the sub-grid scale approach (Mölders et al. 1996; Wang et al. 2006), should be used: For each surface element, a separate multilayer model (often of the Surface-Vegetation-Atmosphere-Transfer type: SVAT) interacting with the neighbourhood grid cell by horizontal fluxes and advection can then be calculated (Fig. 2.14b). The structure of the surface will be



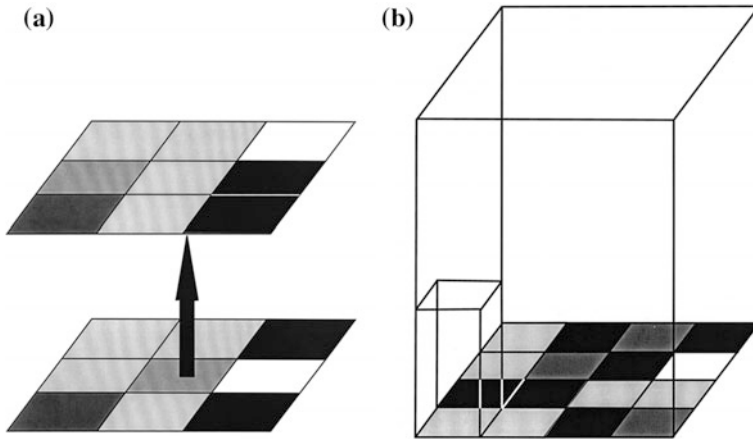


**Fig. 2.14** **a** Schematic figure of the tile approach. The initial distribution of the surface structures will be combined according to their contributions for further calculation. **b** Schematic view of the sub-grid scale (Foken 2008)

not changed and for each surface type a multilayer model will be used which interacts each other by horizontal flow.

A more sophisticated approach to aggregate roughness lengths under consideration of local advection effects was developed by Hasager and Jensen (1999). This microscale aggregation model accounts for the adjustment of the flow to roughness change in arbitrary surface conditions. The physics consists of a linearized version of the atmospheric momentum equation in which only the advective term and the vertical flux divergence are assumed to be of importance, while all other terms such as the Coriolis term are neglected (Hasager et al. 2003). The algorithms are solved by Fast Fourier Transform to allow the time-efficient computation of the effective roughness parameter in accordance with average stress for a given background flow. Terrain information is provided using high-resolution two-dimensional land-use maps, with a fixed roughness length assigned to each land-use class. The application of this method for footprint modeling was demonstrated by Göckede et al. (2006).

Since area averaging of representative surface parameters is usually a pre-processing step to the actual footprint computation, the problem of finding a suitable averaging scheme is more a responsibility of the model user than of the model developer. Accordingly, the use of different aggregation approaches has been published mostly in application papers (Chap. 8). The experimentalist using footprint models must keep in mind that most footprint models are only valid for homogeneous surfaces, and any application in heterogeneous terrain may compromise the model output. The use of averaging techniques to produce aggregated, homogeneous surface fluxes opens footprint models to larger areas of application, but the neglect of high variability of turbulent fluxes at subgrid-scale in the

**Table 2.16** Flux-averaging approaches used in footprint models

Averaging technique	Used in
Homogeneous surface	Schuepp et al. (1990), Leclerc and Thurtell (1990), Horst and Weil (1992, 1994), Schmid (1994, 1997), Flesch (1996), Leclerc et al. (1997), Haenel and Grünhage (1999), Rannik et al. (2000, 2003), Kormann and Meixner (2001) and others
Effective roughness length	Applicable to most models
Effective roughness length according to a momentum flux averaging (Hasager and Jensen 1999)	Göckede et al. (2006) using the model by Rannik et al. (2000, 2003)
Heterogeneous surface	Kljun et al. (2002), Steinfeld et al. (2008), Sogachev and Lloyd (2004)

heterogeneous terrain may significantly bias the computations. Table 2.16 separates the footprint model regarding use for homogeneous or heterogeneous surfaces and summarizes flux aggregation approaches used for footprint models.

## References

- Andreas EL (2002) Parametrizing scalar transfer over snow and ice: a review. *J Hydrometeorol* 3:417–432
- Andreas EL and Cash BA (1999) Convective heat transfer over wintertime leads and polynyas. *J Geophys Res.* 104:15.721–725.734
- Antonia RA, Luxton RE (1971) The response of turbulent boundary layer to a step change in surface roughness, part 1. *J Fluid Mech* 48:721–761
- Antonia RA, Luxton RE (1972) The response of turbulent boundary layer to a step change in surface roughness, part 2. *J Fluid Mech* 53:737–757
- Arya SP (1999) *Air pollution meteorology and dispersion*. Oxford University Press, New York, Oxford, 310 pp
- Arya SP (2001) *Introduction to micrometeorology*. Academic Press, San Diego, 415 pp
- Aubinet M, Vesala T and Papale D (2012) *Eddy covariance: a practical guide to measurement and data analysis*. Springer, Dordrecht, 438 pp
- Baldocchi D (1997) Flux footprints within and over forest canopies. *Bound-Layer Meteorol* 85:273–292
- Behrendt A, Wulfmeyer V, Riede A, Wagner G, Pal S, Bauer H, Radlach M, Späth F (2009) 3-Dimensional observations of atmospheric humidity with a scanning differential absorption lidar. In: Picard RH et al (eds) *Remote sensing of clouds and the atmosphere XIV*, SPIE conference proceeding, vol 7475, Art No 74750L. doi:74710.71117/74712.835143
- Beyrich F et al (2006) Area-averaged surface fluxes over the LITFASS region on eddy-covariance measurements. *Bound-Layer Meteorol* 121:33–65
- Blackadar AK (1997) *Turbulence and Diffusion in the Atmosphere*. Springer, Berlin, 185 pp
- Blöschl G, Sivapalan M (1995) Scale issues in hydrological modelling: a review. *Hydrol Processes* 9:251–290
- Bowen IS (1926) The ratio of heat losses by conduction and by evaporation from any water surface. *Phys Rev* 27:779–787

- Bradley EF (1968) A micrometeorological study of velocity profiles and surface drag in the region modified by change in surface roughness. *Quart J Roy Meteorol Soc* 94:361–379
- Brunet Y, Finnigan JJ, Raupach MR (1994) A wind tunnel study of air flow in waving wheat: single-point velocity statistics. *Bound-Layer Meteorol* 70:95–132
- Businger JA, Yaglom AM (1971) Introduction to Obukhov's paper "Turbulence in an atmosphere with a non-uniform temperature". *Bound-Layer Meteorol* 2:3–6
- Businger JA, Wyngaard JC, Izumi Y, Bradley EF (1971) Flux-profile relationships in the atmospheric surface layer. *J Atmos Sci* 28:181–189
- Cellier P, Brunet Y (1992) Flux-gradient relationships above tall plant canopies. *Agric Forest Meteorol* 58:93–117
- Cionco RM (1978) Analysis of canopy index values for various canopy densities. *Bound-Layer Meteorol* 15:81–93
- Claussen M (1991) Estimation of areally-averaged surface fluxes. *Bound-Layer Meteorol* 54:387–410
- Claussen M (1995) Flux aggregation at large scales: on the limits of validity of the concept of blending height. *J Hydrol* 166:371–382
- Claussen M, Walmsley JL (1994) Modification of blending procedure in a proposed new PBL resistance law. *Bound-Layer Meteorol* 68:201–205
- Davenport AG, Grimmond CSB, Oke TR and Wieringa J (2000) Estimating the roughness of cities and sheltered country. In: 12th conference on applied climatology, Asheville, NC2000. American Meteorological Society, pp 96–99
- Deardorff JW (1972) Numerical investigation of neutral und unstable planetary boundary layer. *J Atmos Sci* 29:91–115
- Denmead DT, Bradley EF (1985) Flux-gradient relationships in a forest canopy. In: Hutchison BA, Hicks BB (eds) *The forest-atmosphere interaction*. D. Reidel Publishing Company, Dordrecht, pp 421–442
- Denmead DT, Bradley EF (1987) On scalar transport in plant canopies. *Irrig Sci* 8:131–149
- Doran JC, Verhokle MG (1978) A note on vertical extrapolation formulas for Weibull velocity distribution parameters. *J Climate Appl Meteorol* 17:410–412
- Draxler RR (1976) Determination of atmospheric diffusion parameters. *Atmos Environ* 10:99–105
- Dupont S, Brunet Y (2009) Coherent structures in canopy edge flow: a large-eddy simulation study. *J Fluid Mech* 630:93–128
- Durden DJ, Nappo CJ, Leclerc MY, Duarte HF, Zhang G, Parker MJ, Kurzeja RJ (2013) On the impact of wave-like disturbances on turbulent fluxes and turbulence statistics in night-time conditions: a case study. *Biogeosci* 10:8433–8443
- Dyer AJ (1974) A review of flux-profile-relationships. *Bound-Layer Meteorol* 7:363–372
- Eigenmann R, Metzger S, Foken T (2009) Generation of free convection due to changes of the local circulation system. *Atmos Chem Phys* 9:8587–8600
- Elliott WP (1958) The growth of the atmospheric internal boundary layer. *Trans Am Geophys Union* 39:1048–1054
- ESDU (1972) Characteristics of wind speed in the lowest layers of the atmosphere near the ground: strong winds. Engineering Science Data Unit Limited. Regent street, London
- Fiedler F, Panofsky HA (1972) The geostrophic drag coefficient and the 'effective' roughness length. *Quart J Roy Meteorol Soc* 98:213–220
- Finnigan J (2000) Turbulence in plant canopies. *Ann Rev Fluid Mech* 32:519–571
- Finnigan JJ, Clement R, Malhi Y, Leuning R, Cleugh HA (2003) A re-evaluation of long-term flux measurement techniques, part I: Averaging and coordinate rotation. *Bound-Layer Meteorol* 107:1–48
- Fitzmaurice L, Shaw RH, Paw UKT, Patton EG (2004) Three-dimensional scalar microfront systems in a large-eddy simulation of vegetation canopy flow. *Bound-Layer Meteorol* 112:107–127
- Flesch TK (1996) The footprint for flux measurements, from backward Lagrangian stochastic models. *Bound-Layer Meteorol* 78:399–404

- Foken T (1990) Turbulenter Energieaustausch zwischen Atmosphäre und Unterlage: Methoden, meßtechnische Realisierung sowie ihre Grenzen und Anwendungsmöglichkeiten. *Ber Dt Wetterdienstes* 180:287 pp
- Foken T (2006) 50 years of the Monin-Obukhov similarity theory. *Bound-Layer Meteorol* 119:431–447
- Foken T (2008) *Micrometeorology*. Springer, Berlin, 308 pp
- Foken T, Wichura B (1996) Tools for quality assessment of surface-based flux measurements. *Agric Forest Meteorol* 78:83–105
- Foken T, Skeib G, Richter SH (1991) Dependence of the integral turbulence characteristics on the stability of stratification and their use for Doppler-Sodar measurements. *Z Meteorol* 41:311–315
- Foken T et al (2012) Coupling processes and exchange of energy and reactive and non-reactive trace gases at a forest site: results of the EGER experiment. *Atmos Chem Phys* 12:1923–1950
- Friedrich K, Mölders N, Tetzlaff G (2000) On the influence of surface heterogeneity on the Bowen-ratio: a theoretical case study. *Theor Appl Clim* 65:181–196
- Frisch U (1995) *Turbulence*. Cambridge University Press, Cambridge, 296 pp
- Garratt JR (1978) Flux profile relations above tall vegetation. *Quart J Roy Meteorol Soc* 104:199–211
- Garratt JR (1980) Surface influence upon vertical profiles in the atmospheric near surface layer. *Quart J Roy Meteorol Soc* 106:803–819
- Garratt JR (1990) The internal boundary layer: a review. *Bound-Layer Meteorol* 50:171–203
- Garratt JR (1992) *The atmospheric boundary layer*. Cambridge University Press, Cambridge, 316 pp
- Gash JHC (1986) A note on estimating the effect of a limited fetch on micrometeorological evaporation measurements. *Bound-Layer Meteorol* 35:409–414
- Geiger R, Aron RH and Todhunter P (2009) *The climate near the ground*. Rowman & Littlefield Publishers, Lanham, 623 pp
- Göckede M, Rebmann C, Foken T (2004) A combination of quality assessment tools for eddy covariance measurements with footprint modelling for the characterisation of complex sites. *Agric Forest Meteorol* 127:175–188
- Göckede M, Markkanen T, Hasager CB, Foken T (2006) Update of a footprint-based approach for the characterisation of complex measuring sites. *Bound-Layer Meteorol* 118:635–655
- Göckede M, Thomas C, Markkanen T, Mauder M, Ruppert J, Foken T (2007) Sensitivity of Lagrangian stochastic footprints to turbulence statistics. *Tellus* 59B:577–586
- Goudriaan J (1977) *Crop micrometeorology: A simulation study*. Center for Agricultural Publishing and Documentation, Wageningen, 249 pp
- Graefe J (2004) Roughness layer corrections with emphasis on SVAT model applications. *Agric Forest Meteorol* 124:237–251
- Grimmond CSB, Oke TR (1999) Aerodynamic properties of urban areas derived from analysis of surface form. *J Appl Meteorol* 38:1262–1292
- Grimmond CSB, King TS, Roth M, Oke TR (1998) Aerodynamic roughness of urban areas derived from wind observations. *Bound-Layer Meteorol* 89:1–24
- Gryning S-E, van Ulden AP, Larsen S (1983) Dispersions from a ground level source investigated by a K model. *Quart J Roy Meteorol Soc* 109:355–364
- Gryning SE, Holtslag AAM, Irvin JS, Sivertsen B (1987) Applied dispersion modelling based on meteorological scaling parameters. *Atmos Environ* 21:79–89
- Haenel H-D, Grünhage L (1999) Footprint analysis: a closed analytical solution based on height-dependent profiles of wind speed and eddy viscosity. *Bound-Layer Meteorol* 93:395–409
- Handorf D, Foken T, Kottmeier C (1999) The stable atmospheric boundary layer over an Antarctic ice sheet. *Bound-Layer Meteorol* 91:165–186
- Harman IN, Finnigan JJ (2007) A simple unified theory for flow in the canopy and roughness sublayer. *Bound-Layer Meteorol* 123:339–363
- Harman IN, Finnigan JJ (2008) Scalar concentration profiles in the canopy and roughness sublayer. *Bound-Layer Meteorol* 129:323–351

- Hasager CB, Jensen NO (1999) Surface-flux aggregation in heterogeneous terrain. *Quart J Roy Meteorol Soc* 125:2075–2102
- Hasager CB, Nielsen NW, Jensen NO, Boegh E, Christensen JH, Dellwik E, Soegaard H (2003) Effective roughness calculated from satellite-derived land cover maps and hedge-information used in a weather forecasting model. *Bound-Layer Meteorol* 109:227–254
- Hatfield JL and Baker JM (eds) (2005) *Micrometeorology in agricultural systems*. American Society of Agronomy, Madison, 584 pp
- Hicks BB (1981) An examination of the turbulence statistics in the surface boundary layer. *Bound-Layer Meteorol* 21:389–402
- Högström U (1988) Non-dimensional wind and temperature profiles in the atmospheric surface layer: a re-evaluation. *Bound-Layer Meteorol* 42:55–78
- Högström U (1990) Analysis of turbulence structure in the surface layer with a modified similarity formulation for near neutral conditions. *J Atmos Sci* 47:1949–1972
- Högström U (1996) Review of some basic characteristics of the atmospheric surface layer. *Bound-Layer Meteorol* 78:215–246
- Högström U, Hunt JCR, Smedman A-S (2002) Theory and measurements for turbulence spectra and variances in the atmospheric neutral surface layer. *Bound-Layer Meteorol* 103:101–124
- Horst TW (1979) Lagrangian similarity modeling of vertical diffusion from a ground level source. *J Appl Meteorol* 18:733–740
- Horst TW (1999) The footprint for estimation of atmosphere-surface exchange fluxes by profile techniques. *Bound-Layer Meteorol* 90:171–188
- Horst TW (2000) An intercomparison of measures of special inhomogeneity for surface fluxes of passive scalars. In: 14th symposium on boundary layer and turbulence, Aspen CO, 7–11 August 2000. American Meteorological Society, pp 11–14
- Horst TW, Weil JC (1992) Footprint estimation for scalar flux measurements in the atmospheric surface layer. *Bound-Layer Meteorol* 59:279–296
- Horst TW, Weil JC (1994) How far is far enough?: the fetch requirements for micrometeorological measurement of surface fluxes. *J Atm Oceanic Tech* 11:1018–1025
- Hsieh C-I, Katul G (2009) The Lagrangian stochastic model for estimating footprint and water vapor fluxes over inhomogeneous surfaces. *Int J Biometeorol* 53:87–100
- Hsieh C-I, Katul G, Chi T-W (2000) An approximate analytical model for footprint estimation of scalar fluxes in thermally stratified atmospheric flows. *Adv Water Res* 23:765–772
- Hsu SA, Meindl EA, Gilhousen DB (1994) Determination of power-law wind-profile exponent under near: neutral stability conditions at sea. *J Appl Meteorol* 33:757–765
- Huang CH (1979) A theory of dispersion in turbulent shear flow. *Atmos Environ* 13:453–463
- Irvin JS (1978) A theoretical variation of the wind profile power-law exponent as a function of surface roughness and stability. *Atmos Environ* 13:191–194
- Jegede OO, Foken T (1999) A study of the internal boundary layer due to a roughness change in neutral conditions observed during the LINEX field campaigns. *Theor Appl Clim* 62:31–41
- Joffre SM (1984) Power laws and the empirical representation of velocity and directional shear. *J Clim Appl Meteorol* 23:1196–1203
- Johansson C, Smedman A, Högström U, Brasseur JG, Khanna S (2001) Critical test of Monin-Obukhov similarity during convective conditions. *J Atmos Sci* 58:1549–1566
- Kader BA, Yaglom AM (1972) Heat and mass transfer laws for fully turbulent wall flows. *Int J Heat Mass Transf* 15:2329–2350
- Kaharabata SK, Schuepp PH, Ogunjemiyo S, Shen S, Leclerc MY, Desjardins RL, MacPherson JJ (1997) Footprint considerations in BOREAS. *J Geophys Res* 102(D24):29113–29124
- Kaimal JC and Finnigan JJ (1994) *Atmospheric boundary layer flows: their structure and measurement*. Oxford University Press, New York, 289 pp
- Kaimal JC, Gaynor JE (1991) Another look to sonic thermometry. *Bound-Layer Meteorol* 56:401–410
- Kanda M, Moriwaki R, Roth M, Oke T (2002) Area-averaged sensible heat flux and a new method to determine zero-plane displacement length over an urban surface using scintillometry. *Bound-Layer Meteorol* 105:177–193

- Klaassen W, Sogatchev A (2006) Flux footprint simulation downwind of a forest edge. *Bound-Layer Meteorol* 121:459–473
- Klaassen W, van Breugel PB, Moors EJ, Nieveen JP (2002) Increased heat fluxes near a forest edge. *Theor Appl Clim* 72:231–243
- Kljun N, Rotach MW, Schmid HP (2002) A three-dimensional backward Lagrangian footprint model for a wide range of boundary layer stratification. *Bound-Layer Meteorol* 103:205–226
- Koeltzsch K (1999) On the relationship between the Lagrangian and Eulerian time scale. *Atmos Environ* 33:117–128
- Kolmogorov AN (1941a) Lokalnaja struktura turbulentnosti v neschtschimaemoi schidkosti pri otschen bolschich tschislach Reynoldsa (The local structure of turbulence in incompressible viscous fluid for very large Reynolds numbers). *Dokl AN SSSR* 30:299–303
- Kolmogorov AN (1941b) Rassejanie energii pri lokalno-isotropoi turbulentnosti (Dissipation of energy in locally isotropic turbulence). *Dokl AN SSSR* 32:22–24
- Kormann R, Meixner FX (2001) An analytical footprint model for non-neutral stratification. *Bound-Layer Meteorol* 99:207–224
- Leclerc MY, Thurtell GW (1990) Footprint prediction of scalar fluxes using a Markovian analysis. *Bound-Layer Meteorol* 52:247–258
- Leclerc MY, Beissner KC, Shaw RH, den Hartog G, Neumann HH (1990) The influence of atmospheric stability on the budgets of the Reynolds stress and turbulent kinetic energy within and above a deciduous forest. *J Appl Meteorol* 29:916–933
- Leclerc MY, Beissner KC, Shaw RH, den Hartog G, Neumann HH (1991) The influence of buoyancy on third-order turbulent velocity statistics within a deciduous forest. *Bound-Layer Meteorol* 55:109–123
- Leclerc MY, Shen S, Lamb B (1997) Observations and large-eddy simulation modeling of footprints in the lower convective boundary layer. *J Geophys Res* 102(D8):9323–9334
- Luhar AK, Rao KS (1994) Source footprint analysis for scalar fluxes measured in flows over an inhomogeneous surface. In: Gryning SE, Millan MM (eds) *Air pollution modeling and its applications*. Plenum Press, New York, pp 315–323
- Lumley JL and Panofsky HA (1964) *The structure of atmospheric turbulence*. Interscience Publishers, New York, 239 pp
- MacDonald RW, Griffiths RF, Hall DJ (1998) An improved method for the estimation of surface roughness of obstacle arrays. *Atmos Environ* 32:1857–1864
- Mahrt L (1996) The bulk aerodynamic formulation over heterogeneous surfaces. *Bound-Layer Meteorol* 78:87–119
- Mao S, Leclerc MY, Michaelides EE (2008) Passive scalar flux footprint analysis over horizontally inhomogeneous plant canopy using large-eddy simulation. *J Atmos Sci* 42:5446–5458
- Markkanen T, Steinfeld G, Kljun N, Raasch S, Foken T (2010) A numerical case study on footprint model performance under inhomogeneous flow conditions. *Meteorol Z* 19:539–547
- Mason PJ (1988) The formation of areally-averaged roughness length. *Quart J Roy Meteorol Soc* 114:399–420
- Mason PJ (1989) Large-eddy simulation of convective atmospheric boundary layer. *J Atmos Sci* 46:1492–1516
- Massman WJ, Weil JC (1999) An analytical one-dimensional second-order closure model of turbulence statistics and the Lagrangian time scale within and above plant canopies of arbitrary structure. *Bound-Layer Meteorol* 91:81–107
- Moene AF, van Dam JC (2014) *Transport in the atmosphere-vegetation-soil continuum*. Cambridge University Press, Cambridge, 436 pp
- Moeng C (1984) A large-eddy simulation model for the study of planetary boundary-layer turbulence. *J Atmos Sci* 41:2052–2062
- Moeng C, Wyngaard JC (1988) Spectral analysis of large-eddy simulations of the convective boundary layer. *J Atmos Sci* 45:3573–3587
- Mölder M, Grelle A, Lindroth A, Halldin S (1999) Flux-profile relationship over a boreal forest: roughness sublayer correction. *Agric Forest Meteorol* 98–99:645–648

- Mölders N, Raabe A, Tetzlaff G (1996) A comparison of two strategies on land surface heterogeneity used in a mesoscale  $\beta$  meteorological model. *Tellus* 48A:733–749
- Monin AS, Obukhov AM (1954) Osnovnye zakonomernosti turbulentnogo peremesivaniya v prizemnom sloe atmosfery (Basic laws of turbulent mixing in the atmosphere near the ground). *Trudy geofiz inst AN SSSR* 24(151):163–187
- Monin AS and Yaglom AM (1973) *Statistical fluid mechanics: mechanics of turbulence*, Volume 1. MIT Press, Cambridge, 769 pp
- Monin AS and Yaglom AM (1975) *Statistical fluid mechanics: mechanics of turbulence*, Volume 2. MIT Press, Cambridge, 874 pp
- Monteith JL, Unsworth MH (2008) *Principles of environmental physics*, 3rd edn. Elsevier, Academic Press, Amsterdam, Boston, 418 pp
- Obukhov AM (1946) Turbulentnost' v temperaturnoj: neodnorodnoj atmosfere (Turbulence in an atmosphere with a non-uniform temperature). *Trudy Inst Theor Geofiz AN SSSR* 1:95–115
- Obukhov AM (1960) O strukture temperaturnogo polja i polja skorostej v uslovijach konvekcii (Structure of the temperature and velocity fields under conditions of free convection). *Izv AN SSSR, ser Geofiz*, 1392–1396
- Obukhov AM (1971) Turbulence in an atmosphere with a non-uniform temperature. *Bound-Layer Meteorol* 2:7–29
- Orlanski I (1975) A rational subdivision of scales for atmospheric processes. *Bull Am Meteorol Soc* 56:527–530
- Panin GN, Tetzlaff G, Raabe A, Schönfeld H-J, Nasonov AE (1996) Inhomogeneity of the land surface and the parametrization of surface fluxes: a discussion. *Wiss Mitt Inst Meteorol Univ Leipzig und Inst Troposphärenforschung Leipzig* 4:204–215
- Panofsky HA (1984) Vertical variation of roughness length at the boulder atmospheric observatory. *Bound-Layer Meteorol* 28:305–308
- Panofsky HA, Tennekes H, Lenschow DH, Wyngaard JC (1977) The characteristics of turbulent velocity components in the surface layer under convective conditions. *Bound-Layer Meteorol* 11:355–361
- Pasquill F (1961) Estimation of the dispersion of windborne material. *Meteorol Mag* 90:33–49
- Pasquill F (1972) Some aspects of boundary layer description. *Quart J Roy Meteorol Soc* 98:469–494
- Pasquill F, Smith FB (1983) *Atmospheric diffusion*, 3rd edn. Wiley, Chichester
- Patton EG, Davis KJ, Barth MC, Sullivan PP (2001) Decaying scalars emitted by a forest canopy: a numerical study. *Bound-Layer Meteorol* 100:91–192
- Paulson CA (1970) The mathematical representation of wind speed and temperature profiles in the unstable atmospheric surface layer. *J Clim Appl Meteorol* 9:857–861
- Peltier LJ, Wyngaard JC, Khanna S, Brasseur JG (1996) Spectra in the unstable surface layer. *J Atmos Sci* 53:49–61
- Peterson EW, Hennessey Jr JP (1978) On the use of power laws for estimates of wind power potential. *J Clim Appl Meteorol* 17:390–394
- Prandtl L (1925) Bericht über Untersuchungen zur ausgebildeten Turbulenz. *Z angew Math Mech* 5:136–139
- Raabe A (1983) On the relation between the drag coefficient and fetch above the sea in the case of off-shore wind in the near shore zone. *Z Meteorol* 33:363–367
- Rannik Ü, Aubinet M, Kurbanmuradov O, Sabelfeld KK, Markkanen T, Vesala T (2000) Footprint analysis for measurements over heterogeneous forest. *Bound-Layer Meteorol* 97:137–166
- Rannik Ü, Markkanen T, Raittila T, Hari P, Vesala T (2003) Turbulence statistics inside and above forest: influence on footprint prediction. *Bound-Layer Meteorol* 109:163–189
- Rao KS, Wyngaard JC, Coté OR (1974) The structure of the two-dimensional internal boundary layer over a sudden change of surface roughness. *J Atmos Sci* 31:738–746
- Raupach MR (1994) Simplified expressions for vegetation roughness length and zero-plane displacement as functions of canopy height and area index. *Bound-Layer Meteorol* 71:211–216

- Raupach MR, Legg BJ (1984) The uses and limitations of flux-gradient relationships in micrometeorology. *Agric Water Manag* 8:119–131
- Raupach MR, Thom AS, Edwards I (1980) A wind-tunnel study of turbulent flow close to regularly arrayed rough surface. *Bound-Layer Meteorol* 18:373–379
- Raupach MR, Coppin PA, Legg BJ (1986) Experiments on scalar dispersion within a model plant canopy. Part I: The turbulence structure. *Bound-Layer Meteorol* 35:21–52
- Raupach MR, Finnigan JJ, Brunet Y (1996) Coherent eddies and turbulence in vegetation canopies: the mixing-layer analogy. *Bound-Layer Meteorol* 78:351–382
- Raynor GS, Michael P, Brown RM, SethuRaman S (1975) Studies of atmospheric diffusion from a nearshore oceanic site. *J Clim Appl Meteorol* 14:1080–1094
- Reithmaier LM, Göckede M, Markkanen T, Knohl A, Churkina G, Rebmann C, Buchmann N, Foken T (2006) Use of remotely sensed land use classification for a better evaluation of micrometeorological flux measurement sites. *Theor Appl Clim* 84:219–233
- Richardson LF (1920) The supply of energy from and to atmospheric eddies. *Proc Roy Soc A* 97:354–373
- Rotach MW, Gryning S-E, Tassone C (1996) A two-dimensional Lagrangian stochastic dispersion model for daytime conditions. *Quart J Roy Meteorol Soc* 122:367–389
- Roth M, Salmond J, Satyanarayana A (2006) Methodological considerations regarding the measurement of turbulent fluxes in the urban roughness sublayer: the role of scintillometry. *Bound-Layer Meteorol* 121:351–375
- Savelyev SA, Taylor PA (2001) Notes on an internal boundary-layer height formula. *Bound-Layer Meteorol* 101:293–301
- Savelyev SA, Taylor PA (2005) Internal boundary layers: I. Height formulae for neutral and diabatic flow. *Bound-Layer Meteorol* 115:1–25
- Schlichting H and Gersten K (2003) *Boundary-layer theory*. McGraw Hill, New York, XXIII, 799 pp
- Schmid HP (1994) Source areas for scalars and scalar fluxes. *Bound-Layer Meteorol* 67:293–318
- Schmid HP (1997) Experimental design for flux measurements: matching scales of observations and fluxes. *Agric Forest Meteorol* 87:179–200
- Schmid HP, Bünzli D (1995a) The influence of the surface texture on the effective roughness length. *Quart J Roy Meteorol Soc* 121:1–21
- Schmid HP, Bünzli D (1995b) Reply to comments by E. M. Blyth on ‘The influence of surface texture on the effective roughness length’. *Quart J Roy Meteorol Soc* 121:1173–1176
- Schmid HP, Oke TR (1990) A model to estimate the source area contributing to turbulent exchange in the surface layer over patchy terrain. *Quart J Roy Meteorol Soc* 116:965–988
- Schoonmaker PK (1998) Paleoecological perspectives on ecological scales. In: Peterson DL, Parker VT (eds) *Ecological scale*. Columbia University Press, New York, pp 79–103
- Schuepp PH, Leclerc MY, MacPherson JJ, Desjardins RL (1990) Footprint prediction of scalar fluxes from analytical solutions of the diffusion equation. *Bound-Layer Meteorol* 50:355–373
- Sedefian L (1980) On the vertical extrapolation of mean wind power density. *J Clim Appl Meteorol* 19:488–493
- Seginer I, Mulhearn PJ, Bradley EF, Finnigan JJ (1976) Turbulent flow in a model plant canopy. *Bound-Layer Meteorol* 10:423–453
- Seibert P, Beyrich F, Gryning S-E, Joffre S, Rasmussen A, Tercier P (2000) Review and intercomparison of operational methods for the determination of the mixing height. *Atmos Environ* 34:1001–1027
- Shaw RH, Patton EG (2003) Canopy element influences on resolved- and subgrid-scale energy within a large-eddy simulation. *Agric Forest Meteorol* 115:5–17
- Shaw RH, Schumann U (1992) Large-eddy simulation of turbulent flow above and within a forest. *Bound-Layer Meteorol* 61:47–64
- Shaw RH, Silversides RH, Thurtell GW (1974) Some observations of turbulence and turbulent transport within and above plant canopies. *Bound-Layer Meteorol* 5:429–449



- Shaw RH, den Hartog G, Neumann HH (1988) Influence of foliar density and thermal stability on profiles of Reynolds stress and turbulence intensity in a deciduous forest. *Bound-Layer Meteorol* 45:391–409
- Shen S, Leclerc MY (1994) Large-eddy simulation of small scale surface effects on the convective boundary layer structure. *Atmos Ocean* 32:717–731
- Shen S, Leclerc MY (1995) How large must surface inhomogeneous be before they influence the convective boundary layer structure? a case study. *Quart J Roy Meteorol Soc* 121:1209–1228
- Shen S, Leclerc MY (1997) Modelling the turbulence structure in the canopy layer. *Agric Forest Meteorol* 87:3–25
- Shir CC (1972) A numerical computation of the air flow over a sudden change of surface roughness. *J Atmos Sci* 29:304–310
- Shuttleworth WJ (1989) Micrometeorology of temperate and tropical forest. *Phil Trans R Soc London B* 324:299–334
- Simpson JJ, Thurtell GW, Neumann HH, Hartog GD, Edwards GC (1998) The validity of similarity theory in the roughness sublayer above forests. *Bound-Layer Meteorol* 87:69–99
- Smedman A-S (1991) Some turbulence characteristics in stable atmospheric boundary layer flow. *J Atmos Sci* 48:856–868
- Sogachev A, Leclerc MY (2011) On concentration footprints for a tall tower in the presence of a nocturnal low-level jet. *Agric Forest Meteorol* 151:755–764
- Sogachev A, Lloyd J (2004) Using a one-and-a-half order closure model of atmospheric boundary layer for surface flux footprint estimation. *Bound-Layer Meteorol* 112:467–502
- Sogachev A, Panferov O (2006) Modification of two-equation models to account for plant drag. *Bound-Layer Meteorol* 121:229–266
- Sogachev A, Menzhulin G, Heimann M, Lloyd J (2002) A simple three dimensional canopy-planetary boundary layer simulation model for scalar concentrations and fluxes. *Tellus* 54B:784–819
- Sogachev A, Leclerc MY, Zhang G, Rannik U, Vesala T (2008) CO<sub>2</sub> fluxes near a forest edge: a numerical study. *Ecol Appl* 18:1454–1469
- Sorbjan Z (1989) Structure of the atmospheric boundary layer. Prentice Hall, New York, 317 pp
- Steinfeld G, Raasch S, Markkanen T (2008) Footprints in homogeneously and heterogeneously driven boundary layers derived from a Lagrangian stochastic particle model embedded into large-eddy simulation. *Bound-Layer Meteorol* 129:225–248
- Stull RB (1988) An introduction to boundary layer meteorology. Kluwer Academic Publisher, Dordrecht, 666 pp
- Stull RB (2000) Meteorology for scientists and engineers. Brooks/Cole, Pacific Grove, 502 pp
- Stull R, Santoso E (2000) Convective transport theory and counter-difference fluxes. In: 14th symposium on boundary layer and turbulence, Aspen, CO., 7–11 August 2000. American Meteorological Society, Boston, pp 112–113
- Su H-B, Leclerc MY (1998) Large-eddy simulation of trace gas footprints from infinite crosswind line sources inside a forest canopy. In: 23th symposium on agricultural and forest meteorology 1998. American Meteorological Society, Boston, pp 388–391
- Su H-B, Shaw RH, Paw UKT, Moeng C-H, Sullivan PP (1998) Turbulent statistics of neutrally stratified flow within and above sparse forest from large-eddy simulation and field observations. *Bound-Layer Meteorol* 88:363–397
- Sullivan PP, Horst TW, Lenschow DH, Moeng C-H, Weil JC (2003) Structure of subfilter-scale fluxes in the atmospheric surface layer with application to large-eddy simulation modelling. *J Fluid Mech* 482:101–139
- Taylor GI (1923) Stability of a viscous liquid contained between two rotating cylinders. *Phil Trans R Soc London* 223:289–343
- Taylor GI (1938) The spectrum of turbulence. *Proc Roy Soc London A* 164:476–490
- Taylor PA (1987) Comments and further analysis on the effective roughness length for use in numerical three-dimensional models: a research note. *Bound-Layer Meteorol* 39:403–418

- Tennekes H (1982) Similarity relations, scaling laws and spectral dynamics. In: Nieuwstadt FTM, Van Dop H (eds) *Atmospheric turbulence and air pollution modelling*. D. Reidel Publishing Company, Dordrecht, pp 37–68
- Thomas C, Foken T (2002) Re-evaluation of integral turbulence characteristics and their parameterisations. In: 15th conference on turbulence and boundary layers, Wageningen, 15–19 July 2002. American Meteorological Society, pp 129–132
- Thomson DJ (1987) Criteria for the selection of stochastic models of particle trajectories in turbulent flows. *J Fluid Mech* 189:529–556
- Thurtell GW (1988) Canopy transport processes: commentary. In: Steffen WL, Denmead OT (eds) *Flow and transport in the natural environment: advances and applications*. Springer, Berlin, pp 128–132
- Tillman JE (1972) The indirect determination of stability, heat and momentum fluxes in the atmospheric boundary layer from simple scalar variables during dry unstable conditions. *J Clim Appl Meteorol* 11:783–792
- Troen I, Peterson EW (1989) *European wind Atlas*. Risø National Laboratory, Roskilde, 656 pp
- van Ulden AP (1978) Simple estimates for vertical diffusion from sources near the ground. *Atmos Environ* 12:2125–2129
- Verhoef A, McNaughton KG, Jacobs AFG (1997) A parameterization of momentum roughness length and displacement height for a wide range of canopy densities. *Hydrol Earth Syst Sci* 1:81–91
- Vogel H-J, Roth K (2003) Moving through scales of flow and transport in soil. *J Hydrol* 272:95–106
- Wang WG, Davis KJ, Cook BD, Butler MP, Ricciuto DM (2006) Decomposing CO<sub>2</sub> fluxes measured over a mixed ecosystem at a tall tower and extending to a region: a case study. *J Geophys Res* 111:G02005.02001–G02005.02014
- Watanabe T (2004) Large-eddy simulation of coherent turbulence structures associated with scalar ramps over plant canopies. *Bound-Layer Meteorol* 112:307–341
- Webb EK (1970) Profile relationships: the log-linear range, and extension to strong stability. *Quart J Roy Meteorol Soc* 96:67–90
- Wieringa J (1980) A revaluation of the Kansas mast influence on measurements of stress and cup anemometer overspeeding. *Bound-Layer Meteorol* 18:411–430
- Wieringa J (1989) Shapes of annual frequency distribution of wind speed observed on high meteorological masts. *Bound-Layer Meteorol* 47:85–110
- Wieringa J (1992) Updating the Davenport roughness classification. *J Wind Eng Ind Aerodyn* 41:357–368
- Wilczak JM, Oncley SP, Stage SA (2001) Sonic anemometer tilt correction algorithms. *Bound-Layer Meteorol* 99:127–150
- Wilson JD, Thurtell GW, Kidd GE (1981) Numerical simulation of particle trajectories in inhomogeneous turbulence. II. Systems with variable turbulent velocity scale. *Bound-Layer Meteorol* 21:423–441
- Wilson JD, Ward DP, Thurtell GW, Kidd GE (1982) Statistics of atmospheric turbulence within and above a corn canopy. *Bound-Layer Meteorol* 24:495–519
- Wyngaard JC (2010) *Turbulence in the atmosphere*. Cambridge University Press, Cambridge, 393 pp
- Wyngaard JC, Coté OR (1971) The budgets of turbulent kinetic energy and temperature variance in the atmospheric surface layer. *J Atmos Sci* 28:190–201
- Yaglom AM (1979) Similarity laws for constant-pressure and pressure-gradient turbulent wall flow. *Ann Rev Fluid Mech* 11:505–540
- Yue W, Parlange MB, Meneveau C, Zhu W, van Hout R, Katz J (2007) Large-eddy simulation of canopy flow using plant-scale representation. *Bound-Layer Meteorol* 124:183–203

Footprints in Micrometeorology and Ecology

Leclerc, M.Y.; Foken, Th.

2014, XIX, 239 p. 114 illus., 38 illus. in color., Hardcover

ISBN: 978-3-642-54544-3